Applied Catalysis B: Environmental 260 (2020) 118148

Contents lists available at ScienceDirect

Applied Catalysis B: Environmental

journal homepage: www.elsevier.com/locate/apcatb

The role of metal–support interaction in Ag/CeO_2 catalysts for CO and soot oxidation

M.V. Grabchenko[a], G.V. Mamontov[a], V.I. Zaikovskii[b,c], V. La Parola[d], L.F. Liotta[d], O.V. Vodyankina[a,*]

[a] Tomsk State University, 36, Lenin ave., 634050, Tomsk, Russia
[b] Boreskov Institute of Catalysis, 5, Lavrentiev ave., 630090, Novosibirsk, Russia
[c] Novosibirsk State University, 2, Pirogova Str., 630090, Novosibirsk, Russia
[d] Istituto per lo Studio dei Materiali Nanostrutturati (ISMN)-CNR, 153, via Ugo La Malfa, 90146, Palermo, Italy

ARTICLE INFO

Keywords:
Ag/CeO_2
Metal–support interaction
Epitaxial growth of silver particles
CO oxidation
Soot combustion

ABSTRACT

Ag/CeO_2 catalysts with a silver loading of 10 wt.% have been prepared by three different techniques: impregnation, Ag/CeO_2 (imp), impregnation of prereduced CeO_2, Ag/CeO_2 (red-imp), and co-deposition precipitation, $Ag\text{-}CeO_2$ (co-DP). The features of the prepared composites have been studied by low-temperature N_2 sorption, TGA, XRF, TPR-H_2, TEM HR, XPS and Raman spectroscopy. The Raman and XPS results show that the addition of silver to CeO_2 significantly increases the defectiveness of CeO_2 particles, and such an effect is a function of the preparation method. The $Ag\text{-}CeO_2$ (co-DP) and Ag/CeO_2 (red-imp) catalysts show enhanced interfacial Ag–CeO_2 interaction caused by the epitaxial growth of silver particles (d_{111} = 2.35 Å) on the CeO_2 surface (d_{111} = 3.1 Å) as well as high amount of oxygen vacancies. A morphology-dependent interplay between the oxygen vacancies and the strength of the Ag–CeO_2 interaction has been revealed. Strengthening of the metal–support interaction enhances the catalytic activity of the composites in both CO oxidation and soot combustion.

1. Introduction

Nowadays the problems of emission of harmful compounds from industrial plants and motor vehicles in crowded urban areas are getting more attention, and new solutions for air cleaning are urgently required. The exhaust gases contain different types of hazardous compounds, including carbon monoxide (CO), nitrogen oxides (NO_x), particulate matter (soot), etc., generated during the incomplete combustion [1–4]. The catalytic total oxidation of such organic pollutants to CO_2 and water is the most effective way for their abatement.

Noble metals (Pt, Ru, Pd, Au, Ag, etc.) supported on oxides (ceria, alumina, silica, etc.) are typical deep oxidation catalysts, and their high activity and stability significantly depend on the properties of the support [5–7]. Despite the developed porous structure [7–13] the use of Al_2O_3, SiO_2 and ZSM-5 as supports for such catalysts is not widespread in comparison with the transition metal oxides. Ceria has been widely used as a support for noble metals by the reasons of its unique redox properties and high oxygen storage capacity (OSC) [1,14]. Over the past decades, the metal/ceria catalysts have been widely studied in total oxidation reactions [15,16], composites based on Pd [17–19], Pt [20–22], Ru [23,24], Au [25–27], Ru/CeO_2 [28,29] and Rh [30,31]. Moreover, recently several publications have been devoted to soot combustion over ceria-based catalysts [1,32,33].

As known, it is highly desirable that the oxidation of harmful organic compounds proceeds at low temperature, while accounting for safety, energy-saving purposes, low costs, and environmental friendliness. However, a significant part of the noble-metal-based catalysts cannot be used under real conditions due to high cost (Pd, Pt, Au are used with a loading of 2–10 wt.%). Therefore, the development of high-performance affordable and stable catalysts for low-temperature total oxidation of harmful compounds is still challenging. The efficiency and cost of such catalysts are associated with the proper selection of the type of active components and the preparation method.

The catalytic properties of the supported materials are determined not only by the chemical nature of the catalyst, the particle size and the loading of the active components, but also by their interaction with the support. The latter effect may be defined in terms of metal–support interaction (MSI) defined as "any effect that a support material modifies the performance of a supported metal catalyst via the synthesis process". The enhanced catalytic activity of the catalysts can be achieved by tuning the metal–support interaction in order to provide a synergistic effect between the active sites of the support and noble metal.

* Corresponding authors.
E-mail addresses: leonardafrancesca.liotta@cnr.it (L.F. Liotta), vodyankina_o@mail.ru (O.V. Vodyankina).

https://doi.org/10.1016/j.apcatb.2019.118148
Received 24 July 2019; Received in revised form 26 August 2019; Accepted 31 August 2019
Available online 03 September 2019
0926-3373/ © 2019 Elsevier B.V. All rights reserved.

Liu [34] identified 12 types of metal-support interactions, among which the strong metal–support interaction (SMSI) is of particular interest. In the literature, the role of the SMSI is widely discussed in terms of explaining the catalytic activity and stability of group VIII metals supported on reducible oxides [35]. Nowadays, the term "strong metal–support interaction" (SMSI) was largely extended due to the progress of physical-chemical methods of analysis that allow identifying the structural features of the materials. Based on the nature of the interaction, the SMSIs can be mainly divided into two types: those interactions stemming from electronic defects and those mainly caused by the surface structural defects [34]. The SMSIs of electronic defects have been proved to be capable of anchoring individual atoms tightly either through direct M_2–M_1 bonding or through the formation of M_2–O–M_1, where M_1 and M_2 represent the supported metal atom and the metal cation of the support, respectively. The second type of SMSI, namely structural defects, can be surface steps, coordinately unsaturated sites, surface vacancies or other types of surface defects. The geometric SMSIs are frequently accompanied by the encapsulation of metal particles by oxide support [36].

The SMSI gives rise to three major effects: electronic, geometric and bifunctional, and their combination allowed the author [35] to distinguish between WMSI (weak metal-support interaction) and SMSI. The work function of noble metal is one of the main factors that causes the appearance of the SMSI effect [37]. Indeed, Ag has a work function of 4.26 eV that is lower as compared with 5.65 eV for Pt, but is close to 4.71 eV for Ru, 4.98 eV for Rh [38]. The SMSI effect for Ru-containing catalysts was described in the literature [39,40]. Thus, the decrease of the work function for Ag is not an obstacle for the appearance of the different types of MSI for supported Ag catalysts. Moreover, the work function of the metal depends on the size of its nanoparticles, the presence of impurities, etc. In Ref. [41], the author showed that the clusters of metal atoms (including Ag) provide a significant increase of the ionization energy beyond the bulk work function, when the particle size was reduced. Thus, the MSI is poorly described for Ag catalysts, however, with the decreasing of the sizes of supported Ag particles, the appearance of the enhanced MSI for Ag catalysts can be expected.

In Ref. [42], the geometric effect of the MSI was shown. If the interaction between a metal particle and a support surface is strong, then the growth of the metal particle is controlled by the surface structure of the substrate, and the particle exposes a surface parallel to the substrate irrespective of the anisotropy of the surface energy of the particle facets or the substrate. In this situation, the interfacial adhesion energy is high and the particle is strongly bonded. Small or no mismatch of lattice constants facilitates epitaxial growth. Usually, epitaxial growth can immobilize the metal nanoparticles resulting in a relatively uniform distribution of particles with small sizes. The authors showed a HRTEM image of an Ag/MgO model catalyst clearly revealing the epitaxial growth of the small Ag nanoparticles onto the {100} surfaces of the MgO cubes. *J.* A. Farmer and C. T. Campbell showed the calorimetrically measured adhesion energies of Ag nanoparticles to reduced CeO_{2-x} (111) surfaces and average Ag particle size [43]. These results show that the adhesion energy of Ag nanoparticles to CeO_2 (111) increases with the extent of CeO_2 reduction. The adhesion energies of Ag nanoparticles to these CeO_{2-x} (111) surfaces (~2.3 to 2.6 J/m^2) approach and even exceed the one for Ag–Ag adhesion (twice the surface energy of Ag, 2.44 J/m^2). For the adhesion energy equal to or larger than the Ag–Ag adhesion energy, one would generally not expect the Ag to form a clusters, but instead to wet the surface. However, these results are for local binding of the Ag particle to some part of the ceria surface, where there is likely a much greater defect (vacancy) concentration than elsewhere, and, thus, the local adhesion energy is likely much lower on the stoichiometric CeO_2 terraces. Furthermore, the lattice mismatch between Ag (111) and the underlying CeO_2 (111) will cause the CeO_2 lattice under the Ag island to contract or expand to gain the interfacial bonding stability. It was found that Ag with small sizes has much higher stability on the reduced CeO_2 (111). Thus, these results may explain the unusual MSI for Ag/CeO_2 materials.

However, the role of the MSI in the Ag/CeO_2 catalysts for oxidative processes is practically not discussed. The authors [44] analyzed the experimental dependence of the reduction temperature in TPR-H_2 mode for CeO_2/M/SiO_2 and CeO_2/M/Al_2O_3 samples on the metal work function. The Pt group metals (Pt, Pd, Ru, Rh) as well as Ag and Au were considered. For all samples, the linear dependencies of the reduction temperature on the metal work function were obtained and evidenced similar mechanism of interaction between CeO_2 and metal nanoparticles. However, the catalytic activity of the obtained samples was not studied. The authors [45] showed that due to the MSI effect between the Ag nanoparticles and CeO_2-SBA-15 supports provided by microwave heating, the highly effective catalysts were obtained with high TOF values for the 4-nitrophenol reduction. The authors concluded that the strong charge polarization of CeO_2 clusters during the microwave heating process contributed to the precise control of the Ag particle size and the MSIs relative to those obtained through oil-bath heating. In the abovementioned publications, the catalyst composition contained the supports (SiO_2, Al_2O_3 or SBA-15) besides the Ag and CeO_2. Thus, the study of the main features of the Ag–CeO_2 interaction at the stage of formation of the catalysts as well as the changing of their catalytic activity in the context of the MSI effect is a relevant task.

The key features of the silver–ceria interaction are connected with the morphology and size effects of both Ag and CeO_2 particles, chemical and charge state of silver, charge transfer between silver and ceria, type and concentrations of oxygen vacancies in the ceria structure, oxygen species over Ag particles and redox properties that are caused by the interplay between Ag^+/Ag^0 and Ce^{3+}/Ce^{4+} pairs [15]. For this reason, the Ag/CeO_2 is a promising heterogeneous catalyst for oxidation of CO [3,46–48] and soot combustion [49–54] due to its high activity and relatively low cost.

We have recently reported that addition of CeO_2 to Ag/SiO_2 catalysts leads to increased activity in oxidative dehydrogenation of ethanol [55,56], and an enhanced Ag–CeO_2 interfacial interaction provides the increased activity and high acetaldehyde yield at low temperatures [57]. The preparation methods of such catalysts play an important role in controlling the interfacial Ag–CeO_2 interaction and enhancing the catalytic activity.

In the present work, we focus on the role of metal–support interaction in CO oxidation and soot combustion over Ag/CeO_2 catalysts prepared by different techniques. The structural and reduction properties, content and type of oxygen vacancies, surface chemical composition and oxidation state of the prepared Ag/CeO_2 catalysts have been characterized by the low-temperature N_2 sorption, TGA, XRF, TPR-H_2, TEM HR, XPS and Raman spectroscopy methods.

2. Experimental

2.1. Materials

Ceria support was prepared by deposition-precipitation method. Aqueous ammonia (NH_4OH, 25 wt.%) was added dropwise to the aqueous solution of cerium nitrate (III) until pH 12 under intensive stirring. The obtained precipitate was filtered, washed by distilled water, dried at 80 °C during overnight and calcined at 500 °C for 5 h.

Ag/CeO_2 catalysts with a nominal loading of silver equal to10 wt.% were prepared by three different techniques: incipient impregnation, co-precipitation, and impregnation of pre-reduced CeO_2. The support was impregnated with an aqueous solution of silver nitrate followed by drying at 80 °C and calcination at 500 °C in an air flow. This catalyst was designated as Ag/CeO_2 (imp). Co-deposition-precipitation technique with a redox reaction between the Ag (I) and Ce(III) was used [58] to prepare a catalyst with an increased interfacial interaction between the active component and the support. Therefore, an aqueous ammonia solution was slowly dropped into the aqueous solution of cerium nitrate (III) and silver nitrate at room temperature under

stirring. Addition of ammonia led to the formation of $Ce(OH)_3$ and AgOH precipitates. AgOH precipitate rapidly transformed into the $Ag(NH_3)_2^+$ complex. Then the $Ag(NH_3)_2^+$ ions were adsorbed on $Ce(OH)_3$ surface followed by a redox reaction at pH = 12 [59] yielding Ag^0 and $Ce(OH)_4$, according to the reaction:

$$Ce(OH)_3 + Ag(NH_3)_2OH + 2H_2O = Ce(OH)_4 + Ag^0 + 2NH_4OH.$$

The darkening of the solution color indicated that the reaction had occurred. The obtained catalyst was designated as Ag–CeO_2 (co-DP).

The technique of impregnation of the prereduced CeO_2 was used in order to design a catalyst with an enhanced Ag–CeO_2 interfacial interaction. For this purpose, CeO_2 was pre-reduced at 500 °C in H_2/Ar flow to generate Ce^{3+} species on the surface of ceria nanoparticles (NPs). The impregnation of ceria with an aqueous solution of $AgNO_3$ was accompanied by a redox reaction between the surface Ce^{3+} and Ag^+ leading to the formation of the Ag–CeO_2 interface. After the impregnation, Ag/CeO_2 (red-imp) catalyst was dried at 80 °C and calcined at 500 °C in air flow. According to X-ray fluorescence elemental analysis (XRF), the loading of silver in the prepared catalysts amounted to 10–15 wt.%.

2.2. Materials characterization

Elemental analysis of the catalysts was carried out using a X-ray fluorescence wave-dispersive spectrometer (XRF-1800, Shimadzu, Japan). The source was a X-ray tube with a Rh anode, a voltage of 40 kV, a current of 95 mA and a diaphragm of 10 mm.

The specific surface area (S_{BET}) and a pore size distribution of the samples were determined by N_2 sorption at −196 °C using a TriStar II 3020 analyzer (Micromeritics, United States). Prior to the analysis, all samples were outgassed at 200 °C under vacuum for 2 h. The specific surface area was calculated using the Brunauer–Emmett–Teller (S_{BET}) method, the pore size distribution curves and the pore volume values were determined by the Barrett–Joyner–Halenda (BJH) method from the desorption branches of the isotherms.

The XRD patterns were recorded with a Rigaku Miniflex 600 diffractometer (Rigaku, Japan) using CuK_αradiation (λ = 1.5418 Å). The X-ray diffractograms were registered in the range of 10 to 80° (2θ) with a scanning rate of 2°/min. The crystalline phase composition was determined using the ICSD and PDF database, the average crystallite sizes were determined by the Scherrer's equation and the POWDER CELL 2.4 software was used for detailed profile analysis and calculation of the structural parameters.

Structure of samples and features of Ag–CeO_2 interfaces were studied by TEM HR method using the JEM–2200FS microscope (JEOL). The crystal lattice parameters were calculated by Fast Fourier Transform (FTT) using the DigMicrograph (GATAN) software.

The X-ray photoelectron spectroscopy (XPS) analysis was carried out with a VG Microtech ESCA 3000 Multilab equipped with a dual Mg/Al anode. Unmonochromatized Al Kα radiation (1486.6 eV) was used as an excitation source. The sample powders were analyzed as pellets mounted on a double-sided adhesive tape. The pressure in the analysis chamber was in the range of 10^{-8} Torr during the data collection. The constant charging of the samples was removed by referencing all the energies to the C1s 2p set at 285.1 eV arising from the adventitious carbon. Quick scans of Ce3d region were taken prior to each analysis in order to evaluate possible reduction under the beam. Analysis of the peaks was carried out with the CasaXPS software. Atomic concentrations were calculated from the peak intensity using the sensitivity factors provided with the software. The binding energy (BE) values are quoted with a precision of ± 0.15 eV and the atomic percentage with a precision of ± 10%.

Raman spectra were registered at ambient conditions using an InVia confocal Raman microscope (Renishaw, UK). Prior to analyses, the catalysts were preoxidized in a TPO mode from 25 to up to 500 °C with holding at 500 °C for 20 min and prereduced in 10% vol. of H_2 in Ar at a temperature from 25 to up to 200 °C with holding at 200 °C for 20 min. In addition, Raman studies were carried out after CO oxidation.

Oxygen storage capacity (OSC) was measured by thermogravimetric analysis (TGA) with a TGA/DSC1 STAR system Mettler Toledo. The sample (15 mg) was pretreated in N_2 (30 ml min^{-1}) by heating from 25 to up to 500 °C (ramp rate was 10 °C /min) (step 1) and holding time at 500 °C of 15 min (step 2). Then, the sample was cooled down under nitrogen atmosphere up to 150 °C (step 3). At 150 °C, the sample was saturated with pure O_2 (30 ml/min) during 1 h (step 4) and cooled down to 25 °C still under O_2 (step 5). Finally, the sample was treated under N_2 (30 ml/min) heating from room temperature up to 800 °C (ramp rate was 5 °C/min) (step 6). Steps 1, 2 were carried out in order to remove any adsorbed water, oxygen or carbonate species; during the step 3 the sample was stabilized at 150 °C that is a proper temperature for O_2 chemisorption. Steps 4, 5 were aimed to fill the oxygen vacancies; finally, during the step 6, the removal of chemisorbed oxygen species occurred and the weight loss was taken into account in order to evaluate the oxygen vacancies content of the sample.

The reducibility of catalysts was studied by TPR-H_2 using ChemiSorb 2750 (Micromeritics, United States). The gas flow of 10 vol. % H_2 in Ar with a rate of 20 ml/min was passed through the catalysts (~200 mg) under heating from -50 to 900 °C with a heating rate of 10 °C/min. The samples were pretreated in an air flow at 500 °C prior to each TPR experiment.

2.3. Catalytic activity tests

The catalytic properties were studied in CO oxidation at atmospheric pressure in a fixed-bed quartz reactor (internal diameter was 6 mm) with a heating from -50 °C to up to 500 °C with a rate of 10 °C/min in a flow of 0.5 vol.% CO, 4.4 vol.% O_2 and 95.1 vol.% He gas mixture (300 ml/min). The testing was carried out using the "Chemisorb 2750″ chromatograph (Micromeritics, USA) equipped with a gas mass spectrometer UGA-300 (Stanford Research Systems) to control the concentrations of CO (m/z = 28), CO_2 (m/z = 44) and O_2 (m/z = 32). Typically, 0.45 g of the catalysts were preoxidized in air at 500 °C for 10 min prior to the catalytic tests.

The reaction rate (W) and the activation energy (E_a) were estimated for CO conversions for the first and second cycles from 4% (4.5%) to up to 20% using the following formula:

$$W\ (molecules/m^2 \times s) = (C^0_{CO} \times X \times V_{RM})/\ (m \times S_{BET}),$$

where C^0_{CO} is an initial concentration of CO (molecules/cm^3), X is a CO conversion, V_{RM} is a reaction mixture rate (cm^3/s), m is a weight of the sample (g), and S_{BET} is a specific surface area (cm^2/g).

To study the catalytic activity of the samples in soot combustion a simultaneous thermal analysis (STA-TGA) was used. The tests were carried out using the thermogravimeter STA 449F1 ("Netzsch", Germany). A simulated model diesel soot substance was prepared by mixing 5 wt.% carbon black with the prepared catalyst. Prior to soot oxidation, the catalysts were pre-oxidized in a TPO mode from 25 to 500 °C with holding at 500 °C during 20 min. To obtain the tight contact the catalyst and carbon black were intensively mixed using an agate mortar for 10 min. TGA was performed in the temperature range of 100–800 °C and a heating rate of 10 °C/min in an airflow.

3. Results

3.1. Textural and structural properties

The textural properties of the ceria support and Ag catalysts were studied by N_2 sorption at −196 °C. The main textual and structural properties of the samples are summarized in Table 1. The adsorption-desorption isotherms for ceria and Ag-containing catalysts (see Fig. S1, supporting information) are characterized by a hysteresis loop at relative pressures of 0.45-0.9 indicating the mesoporous structure of the

Table 1
Textural and structural properties of CeO_2 and Ag/CeO_2 catalysts.

Sample	Loading,% (XRF)		S_{BET}, m^2/g	Pore volume, cm^3/g	Average pore size, nm	2θ (peak 111 of CeO_2)	$d_{111(CeO2)}$,Å	$D_{(CeO2)}$,nm
	Ag	CeO_2						
CeO_2	–	100	66	0.098	4.8	28.59	3.121	12.5
Ag/CeO_2 (imp)	14.1	85.9	33	0.061	5.2	28.58	3.121	11.4
Ag-CeO_2 (co-DP)	10.2	89.8	16	0.044	7.9	28.48	3.134	14.1
Ag/CeO_2 (red-imp)	15	85	22	0.042	4.1	28.48	3.134	12.3

samples. Ceria support has a specific surface area of 66 m^2/g, a pore volume of 0.098 cm^3/g and a pore size of 4.8 nm. Silver impregnation over ceria decreases the specific surface area to 33 m^2/g and is accompanied by the modification of the porous texture of the Ag/CeO_2 (imp) catalyst (pore volume decreases to 0.061 cm^3/g, when the pore size is 5.2 nm).

The specific surface area (22 m^2/g and 16 m^2/g, respectively), the pore volume (0.04 cm^3/g) for Ag/CeO_2 (red-imp) and Ag-CeO_2 (co-DP) catalysts and also the average pore size (4.1 nm) for Ag/CeO_2 (red-imp) are significantly lower with respect to pure CeO_2 and Ag/CeO_2 (imp). The increase of the pore size (7.9 nm) for Ag-CeO_2 (co-DP) catalyst with a low pore volume in comparison with those values for other catalysts are connected with a larger particle size of the CeO_2. These findings may result from the different preparation methods involving a modification of the textural properties of ceria.

The XRD analysis was used to evaluate the nature of the crystalline phases formed and to calculate the crystallite size according to Scherrer's equation. XRD patterns of the prepared catalysts are shown in Fig. 1. The ceria support and Ag/CeO_2 catalysts are characterized by the reflection peaks typical for the fluorite CeO_2 phase (ICSD #28753) with the reflection peak (111) at around 28.59° 2θ as reported in Table 1. The calculated average crystallite size (D) of CeO_2 ranges between 11 and 14 nm. A significant shift of the diffraction peaks of ceria to lower angle region is observed in the case of Ag-CeO_2 (co-DP) and Ag/CeO_2 (red-imp) (from 28.59° to 28.48° 2θ). Moreover, these catalysts are characterized by an increased value of d_{111} from 3.121 to 3.134 (see Table 1). Such angular shift and the increased value of the distance between (111) planes of CeO_2 can indicate the incorporation of a part of Ag^+ into the ceria lattice [60,61] or a defective structure of the CeO_2 NPs [62]. On the other hand, it is noteworthy that the Ag-containing catalysts show the reflections at 2θ = 38.1° and 44.3° characteristic for metallic Ag particles (PDF 04-0783). Moreover, a shift of the main diffraction peak of silver to lower angle value (from 38.116° to 38.04° 2θ) is observed for the Ag-CeO_2 (co-DP) and Ag/CeO_2 (red-imp) catalysts (see the enlarged parts in Fig. 1). This may result from the expansion of the silver lattice due to the formation of an epitaxial layer.

3.2. TEM and TEM HR

The structure of the catalysts and ceria support, the distribution of silver on the ceria surface and the features of Ag-CeO_2 composites were studied by TEM HR. The CeO_2 support is characterized by a pseudo-spherical shape of the particles with sizes of 5–15 nm (Fig. 2a) that correlates with the XRD data. Fig. 2b shows the TEM HR image of the Ag/CeO_2 (imp) catalyst. Only small silver clusters with the size of 0.5–2 nm are observed on the surface of the CeO_2 support (see Fig. 2b for the FFT patterns of these clusters), and the reflexes with d_{111} = 2.3–2.4 Å and d_{200} = 2.1 Å confirm the correspondence of such clusters to metallic silver.

The silver particles that differ in size and the strength of interaction with the ceria surface are observed (see Fig. 2 and Fig. S2, S3 in Supporting information) for Ag-CeO_2 (co-DP) catalyst. The formation of silver particles with sizes of 3–8 nm is observed (TEM images are not shown). The TEM HR images for the Ag-CeO_2 (co-DP) catalyst shown in Fig. 2c and d evidence the features of the interaction of Ag NPs with CeO_2 in this catalyst. The epitaxial growth of the Ag NPs with sizes of 2–4 nm and interlayer distances of d_{111} = 2.2 Å and d_{200} = 2.06 Å on the surface of CeO_2 with the corresponding interlayer distances of d_{111} = 3.1 Å and d_{200} = 2.7 Å are shown in TEM HR (Fig. 2c). The presence of the epitaxial growth of Ag over CeO_2 in contrast to the large difference of the interlayer distances (25%) indicates strengthening of the metal–support interaction in this catalyst. The TEM HR image in Fig. 2d demonstrates the presence of a high amount of areas with the epitaxial growth of Ag NPs (reflexes with d_{111} = 2.3 Å) on the surface of CeO_2 (d_{111} = 3.1 Å). Thus, TEM results for Ag-CeO_2 (co-DP) catalyst support the occurrence of the enhanced metal–support interaction in this catalyst.

Fig. 3 shows the results of TEM analysis carried out over the Ag/CeO_2 (red-imp) catalysts. Silver NPs on the ceria surface are not observed in TEM images (not presented). The HAADF-STEM images and mapping of Ce and Ag are shown in Fig. 3a–c, respectively. Silver is homogeneously distributed in the catalyst. Small silver clusters with the size of 1 nm are detected in TEM HR images of the catalyst (Fig. 3d and e). From the FFT diffraction images (insertion in TEM HR images in Fig. 3d and e) the small clusters may be unambiguously attributed to

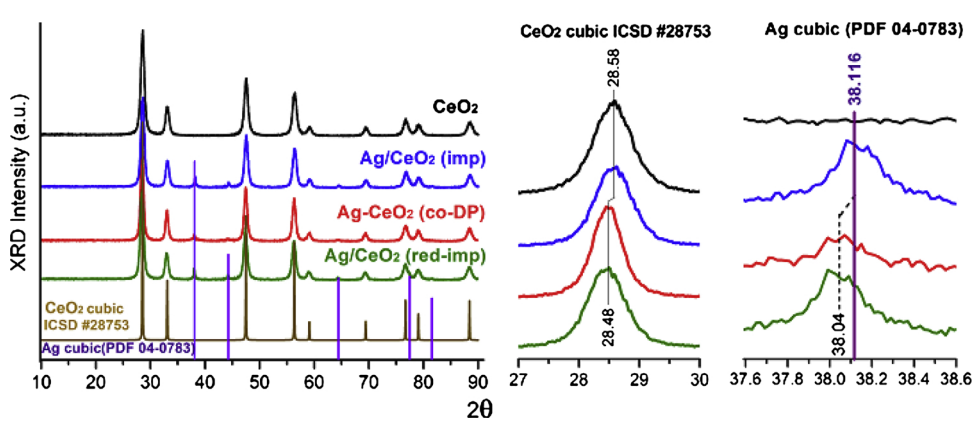

Fig. 1. XRD patterns for CeO_2 and Ag/CeO_2 catalysts.

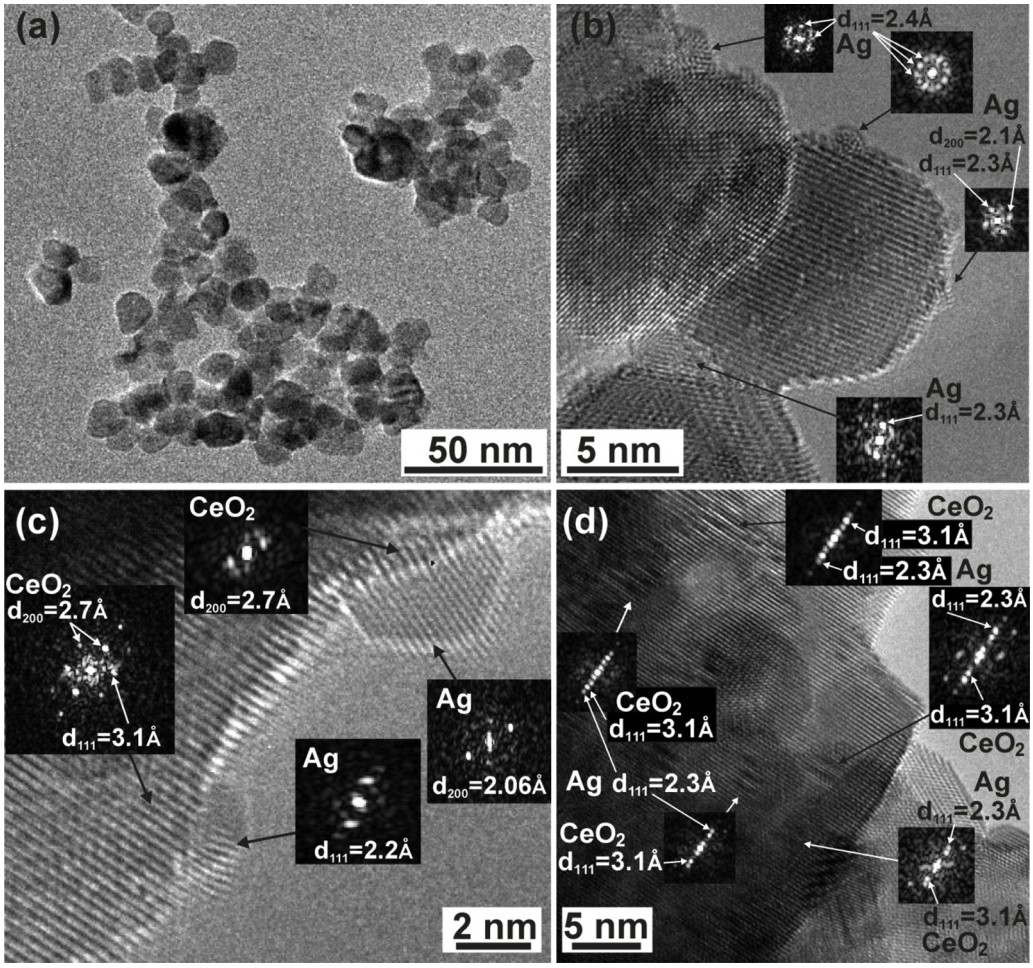

Fig. 2. TEM and TEM HR images of CeO_2 (a), Ag/CeO_2 (imp) (b) and Ag-CeO_2 (co-DP) (c and d) catalysts.

the metallic silver with a lattice parameter $d_{111} \approx 2.3$ Å. The epitaxial growth of the Ag clusters ($d_{111} \approx 2.3$ Å) on the surface of ceria support ($d_{111} \approx 3.1$ Å) is revealed (Fig. 3e) that indicates the enhanced interfacial interaction in this catalyst.

3.3. XPS and Raman results

To study the surface of the catalysts, the XPS analysis was used. Fig. 4a shows the cerium 3d region, and Table 2 contains the percentage of Ce (III) and Ce (IV). In order to check that no artifacts occur due to Ce reduction under the photon beam, a first quick spectrum (recording time was 3 min) of the cerium region was registered and compared to the long acquisition (ca. 2 h) performed afterwards. Only a slight increase of cerium (III) is observed for all samples (see the Fig. 4b for XPS spectrum of CeO_2 as an example), thus, the quick scans have been used for the evaluation of the Ce (III)–Ce (IV) percentage, while the long run has been used to evaluate the surface concentration of the elements.

The complex Ce 3d region has been fitted according to Burroghs et al. [63] with ten components that take into account the spin orbit splitting Ce3d 5/2, Ce 3d 3/2 and other splittings caused by a redistribution of the entire energy spectrum after a core hole is created. There are four peaks (labeled as v^0 u^0, v^i, u^i) attributed to Ce (III) and six peaks (labeled as v, u, v^{ii}, u^{ii}, v^{iii}, u^{iii}) attributed to Ce (IV). The data were fitted using the constraints between the corresponding components 3d5/2- 3d3/2 given by Preisler et al. [64]. The Ce (III) percentages are shown in Table 2 and for all samples range between 22 and 28%. The Ce (III) content decreases from Ag/CeO_2 (imp) to Ag/CeO_2 **(red-i**mp) due to a redox reaction between the surface Ce (III) and Ag^+ yielding the Ag^0–CeO_2 interface. Thus, a part of Ce (III) sites participates in Ag^+ reduction and passes into Ce (IV). The Ce(III) content in CeO_2 sample after in-situ prereduction in XPS pretreatment chamber at 300–350 °C for 18 h or at 500 °C in TPR mode was of only 19 and 18%, respectively. Thus, the calculations of the part of Ce(III) sites participating in the reduction of Ag^+ for Ag/CeO_2 (red-imp) catalyst cannot be carried out correctly because of rapid reoxidation of CeO_2 surface or nonequivalent conditions of reductive pretreatment in TPR mode and in the pretreatment chamber of XPS spectrometer.

Ag 3d region shows an Ag (3d5/2) peak in the region of 368.6–368.9 eV with the splitting of 6 eV for the 3d3/2 doublet. According to Refs. [61–69], the value of Ag (3d5/2) BE of metallic Ag corresponds to 368.0–368.3 eV. The experimentally observed shift towards higher BE region originates from the relaxation of the core hole created by the photoemission, which depends on the shape or/and size of the metal particles [70]. It has been reported that a positive BE shift (+1-2 eV) is connected with highly dispersed particles/clusters supported on oxides [71,72]. In our case, a significant shift to a higher BE (368.9 eV) is observed for Ag/CeO_2 (imp) catalyst and corresponds to small Ag metallic particles. The BE shift from 368.9 eV for Ag/CeO_2 (imp) catalyst to 368.8 and 368.6 eV for Ag-CeO_2 (co-DP) and Ag/CeO_2 (red-imp) catalysts, respectively, may be attributed to an increase of the Ag particle sizes in such an order [72] or/and to a strong electronic metal–support interaction [73–75]. In addition, the shift to lower BEs may be explained as a reverse spillover of oxygen atoms from the Ag – CeO_2 interface to the Ag NPs due to the reduced CeO_2 surface [70]. The formation of Ag_2O is unlikely because in this case a much larger negative shift of BEs of Ag 3d core level (367.6 eV) should be

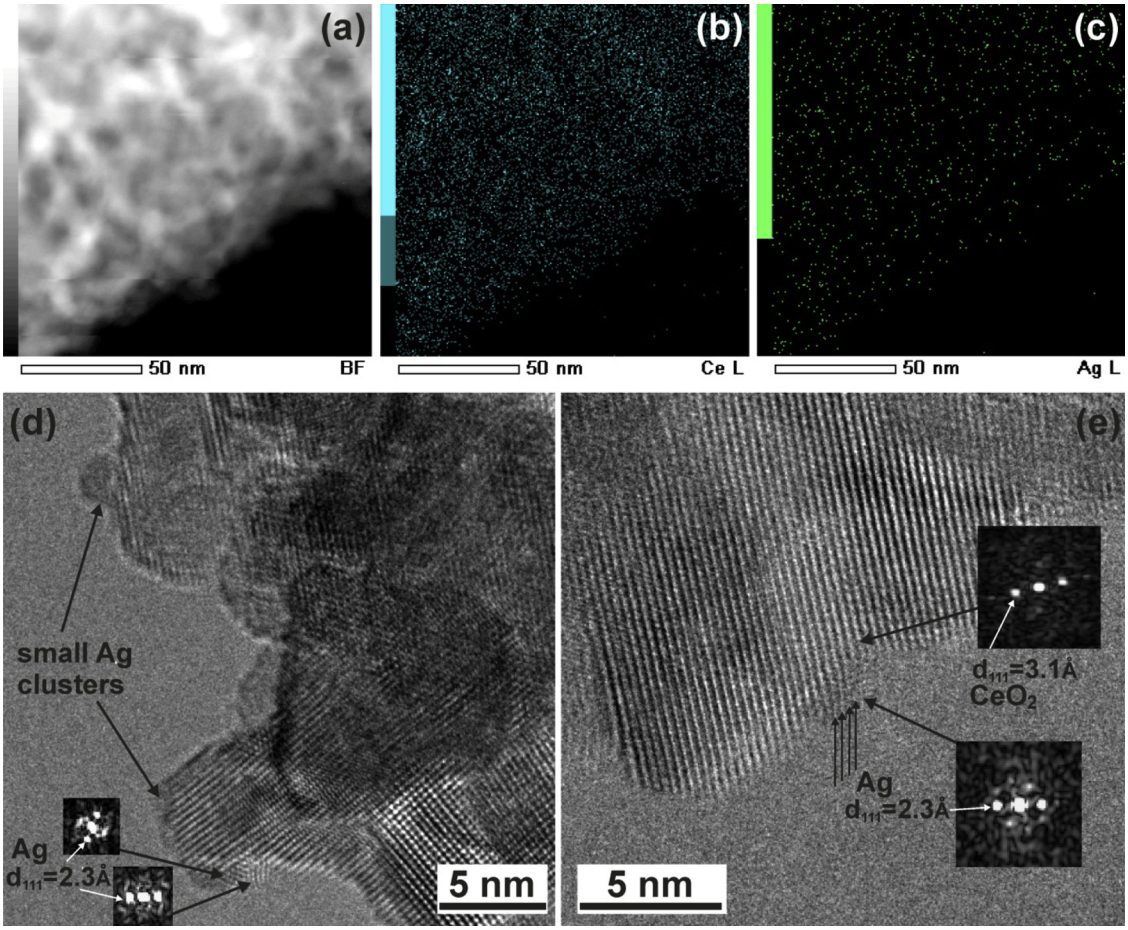

Fig. 3. HAADF-TEM image (a), corresponding distribution of Ce (b) and Ag (c) for this image, and TEM HR images (d and e) of Ag/CeO_2 (red-imp) catalyst.

observed [68,70].

In order to distinguish the chemical species, the Ag MNN Auger regions were recorded and the Auger parameter (AP) were calculated as (Ag3$d_{5/2}$ BE + Ag $M_4N_{4.5}N_{4.5}$ KE) as listed in Table 2. The kinetic energies and the APs (Table 2) for all Ag-containing catalysts differ from the metallic Ag and Ag_2O. According to Refs. [68,76,77], the experimental values of the AP (721.7, 710.8 and 721.4 for Ag/CeO_2 (imp), Ag-CeO_2 (co-DP) and Ag/CeO_2 (red-imp), respectively) may indicate the formation of the oxidized state of Ag (such as in $AgNO_3$) at the Ce-Ag-O interface [78]. This occurs especially in case of co-DP catalyst showing the lowest AP value. Moreover, we cannot exclude that such AP values are due to the formation of transition structures on the boundary between Ag and CeO_2, as it has been observed for Ag/Al_2O_3 [68,77].

Regarding the surface concentration, the impregnated sample (Ag/CeO_2 (imp)) shows the highest amount of surface silver (XPS-derived atomic ratio Ag/Ce is equal to 0.99), while the co-precipitated sample (Ag-CeO_2 (co-DP)) shows the lowest amount of surface silver (Ag/Ce is equal to 0.31). The XPS-derived atomic Ag/Ce ratios (Table 2) were compared with the XRF data. The increase of the Ag/Ce ratio in comparison with the XRF-derived Ag/Ce ratio of Ag/CeO_2 (imp) catalyst confirms the increased amount of silver species on the catalyst surface, while for Ag-CeO_2 (co-DP) and Ag/CeO_2 (red-imp) catalysts, the values of the XPS- and XRF-derived Ag/Ce ratios are relatively close. This finding suggests the uniform distribution of silver both on the surface and in the bulk structure of ceria (incorporation of silver ions onto ceria lattice).

The O1s region is typical for ceria-based materials. According to the literature [79,80], the O1s peaks centered at 529.7, 530.0, and 532.3 eV are assigned to oxygen ions in the CeO_2 lattice, oxygen ions in oxygen-deficient regions within the CeO_2 lattice (the bulk oxygen vacancies), and surface-chemisorbed oxygen species, respectively.

Raman spectroscopy was used to study the lattice oxygen defects and content of oxygen vacancies. Fig. 5a shows the Raman spectra of CeO_2 and Ag/CeO_2 samples prior to CO oxidation. The bands below 200 cm^{-1} can be attributed to particles scattering [81]. The broad bands at around 300 cm^{-1} can be assigned to the displacement of oxygen atoms from the ideal fluorite lattice positions [82]. A strong Raman band at around 465 cm^{-1}, which corresponds to F_{2g} vibration mode of cubic fluoride structure of CeO_2, is observed for CeO_2 sample [83]. The F_{2g} band exhibits the shifts from 465 to 462, 458 and 456 cm^{-1} for Ag/CeO_2 (imp), Ag-CeO_2 (co-DP) and Ag/CeO_2 (red-imp) catalysts, respectively (see the Fig. 5b, where the F_{2g} peak is shown). This red shift suggests defectiveness of ceria structure according to the literature [84]. The broad peak in the region from 500 to 630 cm^{-1} with a maximum at 560 cm^{-1} is characteristic for all Ag-containing catalysts. This defect induced (D_1) mode can be associated with the presence of the bulk oxygen vacancies ($O_{v\text{-}b}$) due to the existence of Ce^{3+} ions and may result from the incorporation of silver ions into the lattice of ceria [46,85,86]. The D_2 peak with a maximum at 950 cm^{-1} observed only for Ag-CeO_2 (co-DP) catalyst can indicate the formation of peroxide species (O-), which may be ascribed to the effect of the high content of surface oxygen vacancies ($O_{v\text{-}s}$) on O_x- [87–89]. The high content of $O_{v\text{-}s}$ vacancies can be related to the presence of the Ce-Ag-O interface proposed based on the AP values.

The intensity ratio of two peaks, I_{D1}/I_{F2g} and I_{D2}/I_{F2g} (I_{F2g} was used as an internal standard), represents the quantitative interpretation of the $O_{v\text{-}b}$ and $O_{v\text{-}s}$ contents, respectively (see Table 3). The I_{D1}/I_{F2g} ratio amount to 0.28, 0.3 and 0.79 for Ag/CeO_2 (imp), Ag-CeO_2 (co-DP) and Ag/CeO_2 (red-imp) catalysts, respectively. The I_{D2}/I_{F2g} ratio amounts to

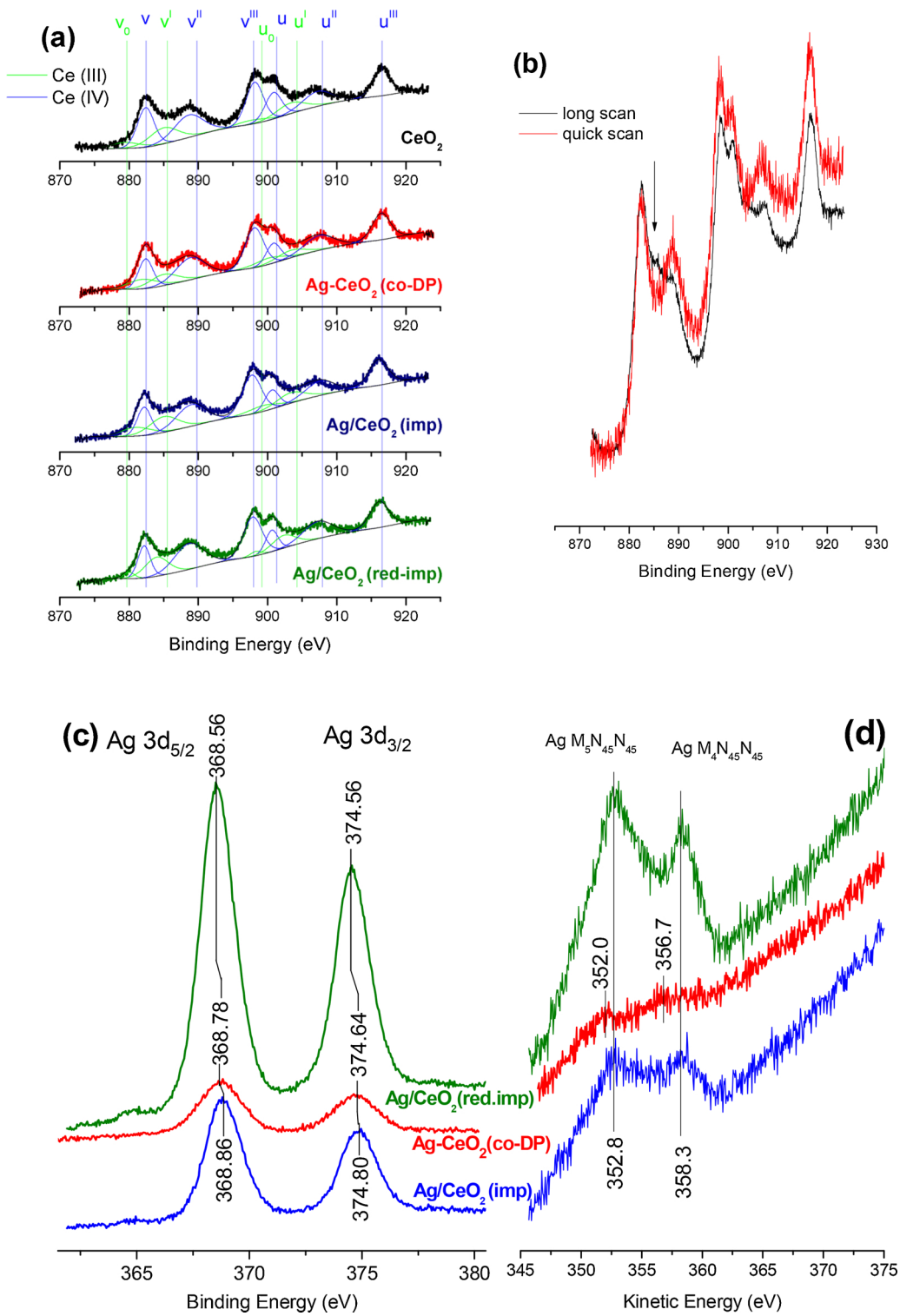

Fig. 4. XPS spectra of Ce3d (a), long and quick scan of Ce3d region of CeO_2 (b), Ag3d (c) and Ag MNN (c) regions of the catalysts.

0.08 and 0.54 for Ag/CeO_2 (imp) and Ag-CeO_2 (co-DP). The calculation of the I_{D2}/I_{F2g} ratio is impossible and is not shown. Additionally, the full width at half maximum of the main peak at 460 cm^{-1} (FWHM) is affected by the amount of oxygen vacancies [90,91]. Thus, a high FWHM value is associated with a high amount of oxygen vacancies in the CeO_2 structure [84]. According to the trend of the FWHM data, the values are equal to 31.5 > 20.9 > 17.5, and the lattice oxygen vacancies increased in the order: Ag-CeO_2 (co-DP) > Ag/CeO_2 (red-imp) > Ag/CeO_2 (imp) and this trend was in agreement with the O1s XPS data (see Table 2). Thus, the Ag-CeO_2 (co-DP) and Ag/CeO_2 (red-imp) are characterized by an increased amount of oxygen vacancies in comparison with the Ag/CeO_2 (imp) catalyst. It is noteworthy that the surface vacancies are predominant for Ag-CeO_2 (co-DP), while an increased amount of bulk vacancies is characteristic for the Ag/CeO_2 (red-imp) catalyst.

Oxygen vacancies were also monitored after the oxidation of CO over CeO_2 and Ag-CeO_2 catalysts. Fig. 5c shows the Raman spectra of the spent catalysts taken after CO oxidation. The spectra are essentially

Table 2
XPS results.

Sample	Ce (III)–Ce (IV)	O1s (eV)	Ag3d5/2 (eV)	AP (eV)	Ag/Ce (XPS)	Ag/Ce (XRF)
CeO_2	22 %-78%	530.0 (80%) 532.6 (20%)	–	–	–	–
Ag/CeO_2 (imp)	28%-72%	530.0 (66%) 532.2 (34%)	368.9	721.7	0.99	0.36
Ag-CeO_2 (co-DP)	26%-7%	529.7 (79%) 532.3 (21%)	368.8	710.8	0.31	0.23
Ag/CeO_2 (red-imp)	22 %-78%	530.0 (71 %) 532.2 (29%)	368.6	721.4	0.46	0.40

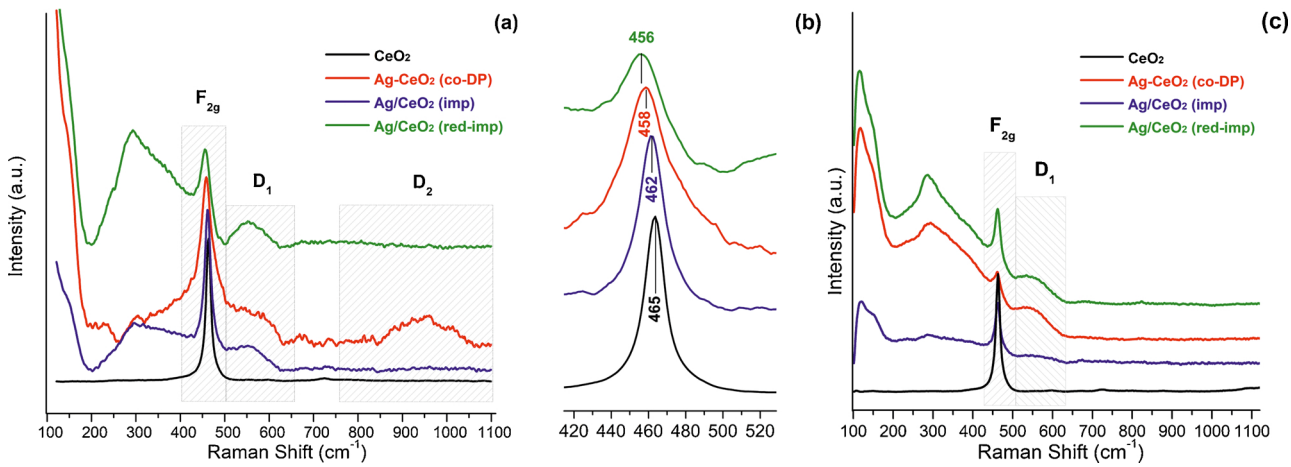

Fig. 5. Raman spectra of CeO_2 and Ag/CeO_2 catalysts: (a, b) after oxidation at 500 °C followed by reduction at 200 °C; (c) spent catalysts after CO oxidation.

the same before and after catalysis. However, the bands (D_2) with a maximum at 950 cm^{-1} are completely eliminated after the CO + O_2 treatment during the catalytic experiment. For all spent catalysts, F_{2g} mode centered at 460 cm^{-1} and the red shift of F_{2g} modes are not observed. The first-order CeO_2 F_{2g} peaks significantly reduce the intensity for spent catalyst as compared to those for the samples before catalysis. The broad bands centered at 560 cm^{-1} (D_1), characterized by the bulk oxygen vacancies, remain for all Ag-containing samples. Such a decrease in intensity of the F_{2g} peaks and a broadening of the D_1 signals are quantitatively related to increase in the amount of bulk oxygen vacancies in the spent catalysts after CO oxidation. This may occur when the reaction is fast (fast reduction and relatively slow reoxidation of the surface), due to the lattice expansion that occurs when Ce^{3+} replaces Ce^{4+} during the oxygen vacancy creation [92]. The intensity ratio of two peaks (I_{D1}/I_{F2g}) are calculated for the spent catalysts (Table 3).

The I_{D1}/I_{F2g} magnitudes are 0.24, 2.02 and 0.68 for Ag/CeO_2 (imp), Ag-CeO_2 (co-DP) and Ag/CeO_2 (red-imp) catalysts, respectively. It was noteworthy that the I_{D1}/I_{F2g} values for Ag/CeO_2 (imp) and Ag/CeO_2 (red-imp) are comparable for fresh and spent catalysts. For the spent Ag-CeO_2 (co-DP) catalyst, a significant increase of bulk oxygen vacancies (for fresh sample the I_{D1}/I_{F2g} was equal to 0.3) is observed. This fact may be explained by migration of the oxygen atoms from the ceria lattice to the surface accompanied by formation of the high concentration of the bulk oxygen vacancies. Under conditions of oxygen excess in the reaction mixture, the disappearance of the surface oxygen vacancies occurs due to the lack of the need to regenerate the own oxygen.

3.4. TPR-H_2 and TGA

The features of the catalyst reduction were studied by the TPR-H_2 method, the results obtained are summarized in Fig. 6 and in Table 4. The TPR profile for CeO_2 is characterized by two regions of hydrogen consumption: the peaks from 350 to 650 °C may be attributed to the reduction of the surface of CeO_2 NPs, while the peak above 750 °C may be associated with the reduction of bulk CeO_2 to Ce_2O_3 [32,93,94]. The area of peaks from 350 to 750 °C corresponds to hydrogen consumption of 145 μmol/g, while for bulk reduction a H_2 consumption of 181 μmol/g is registered.

The TPR-H_2 profiles for Ag-containing catalysts are characterized by few peaks of hydrogen consumption in the temperature range from 0 to 350 °C and high-temperature peaks at 350–750 °C and above 750 °C, respectively. According to the literature [80,89], a reduction peak near

Table 3
Comparison of the catalysts before and after catalysis by Raman spectroscopy and TGA.

Samples	F_{2g} band (cm^{-1})*		I_{D1}/I_{F2g}*		I_{D2}/I_{F2g}*		Weight loss (%)**	
	before	after	before	after	before	after	before	after
CeO_2	465	460	–	–	–	–	–	–
Ag/CeO_2 (imp)	462	460	0.28	0.24	0.08	–	0.47	0.53
Ag-CeO_2 (co-DP)	458	460	0.30	2.02	0.54	–	0.28	0.26
Ag/CeO_2 (red-imp)	456	460	0.79	0.68	–	–	0.28	0.38

*Raman results, **TGA results.

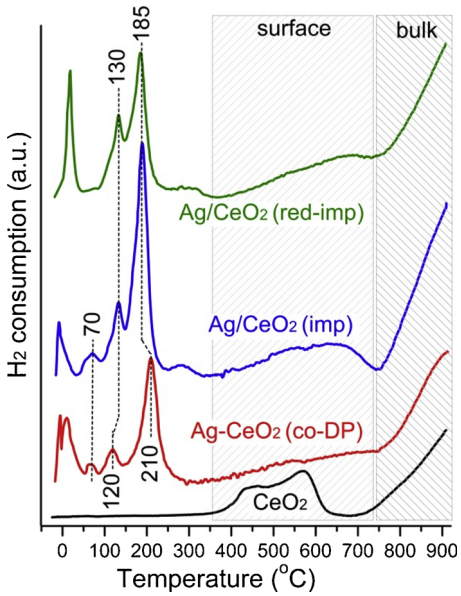

Fig. 6. TPR-H_2 profiles of CeO_2 and Ag/CeO_2 catalysts.

Table 4
Reduction temperatures and H_2 consumption.

Sample	T_{peak}, °C	Peak	H_2 consumed, μmol/g	H_2 consumed, μmol/(m^2)
CeO_2	350-650	surface CeO_2	145	2.2
	750-900	bulk CeO_2	181	2.7
		Σ	326	4.9
Ag/CeO_2 (imp)	0-350	AgO_x and surface CeO_2	395	12.0
	350-750	surface CeO_2	105	3.2
	750-900	bulk CeO_2	409	12.4
		Σ	909	27.5
Ag-CeO_2 (co-DP)	0-350	AgO_x and surface CeO_2	227	14.2
	350-750	surface CeO_2	63	3.9
	750-900	bulk CeO_2	315	19.7
		Σ	605	37.8
Ag/CeO_2 (red-imp)	0-350	AgO_x and surface CeO_2	278	12.6
	350-750	surface CeO_2	54	2.5
	750-900	bulk CeO_2	317	14.4
		Σ	649	29.5

0 °C is assigned to the reduction of O_x– species (O_2– and O–) at the Ag-CeO_2 interface. The H_2 consumption in the temperature region of 0–50 °C increased in the following order: Ag-CeO_2 (co-DP) ≈ Ag/CeO_2 (red-imp) > Ag/CeO_2 (imp). The peak at 70 °C detected for Ag/CeO_2 (imp) and Ag-CeO_2 (co-DP) is associated with the reduction of dispersed silver oxide and/or oxidized silver clusters stabilized on the ceria surface [95]. It is noteworthy that no TPR peak at 70 °C is observed for Ag/CeO_2 (red-imp). The TPR peaks with a maximum at 120–130 °C may be associated with the reduction of silver from the oxidized clusters and highly dispersed silver oxide strongly interacting with ceria surface [57,96,97]. Concerning all Ag samples, the amount of H_2 consumed in this temperature region is less than the theoretical one (ranging between ~1000 and 1300 μmol/g) and is a function of the real silver loading in the catalysts indicated by the XRF results in Table 1). This indicates the presence of both metal and ionic states of silver in Ag/CeO_2 catalysts after the calcination. The presence of metallic silver is also confirmed by the XRD, TEM and XPS analysis.

It is known that the supported noble metals (especially silver) activate surface lattice oxygen in CeO_2 and easily dissociate H_2, greatly facilitating the surface reduction of CeO_2 at low temperatures. Simultaneous decreasing of the intensity of the peak at 350–750 °C in comparison with the pure CeO_2 sample and the presence of the intensive peaks at 185–210 °C for all Ag/CeO_2 catalysts may be attributed to the low-temperature reduction of surface ceria promoted by the silver species. Similar effects were observed for Ag/CeO_2 catalysts in [98], Ag-CeO_2/SiO_2 [55,56], Au/CeO_2 [27], Pt/CeO_2 [99], etc. These results indicate the possibility of simultaneous activation of silver and ceria oxidized species at relatively low temperatures. Thus, the strengthening of the interfacial interactions allows simultaneous reduction of the oxidized silver and ceria.

The highest amount of H_2 consumption in the region of 0–350 °C is obtained for the Ag/CeO_2 (imp) catalysts (395 μmol/g, Table 4). This is attributed to the reduction of highly oxidized silver species that are formed over such a catalyst during the calcination. The relatively high specific surface area (33 m^2/g) and the catalyst preparation method (impregnation with silver nitrate) favor the distribution of the silver precursor mainly on the external surface of ceria generating easily oxidizable species. The TGA curves confirm the highest amount of surface oxygen species released at low temperatures over the Ag/CeO_2 (imp) catalyst.

Conversely, the relatively small amount of the consumed hydrogen registered for the Ag-CeO_2 (co-DP) and Ag/CeO_2 (red-imp) catalysts may result from both a decreased specific surface area (16 and 22 m^2/g, respectively) and high amount of metallic silver due to redox reaction between Ce^{3+} and Ag^+ during the synthesis of the catalysts.

A comparison of the amount of low-temperature consumed hydrogen per specific surface area for the investigated catalysts shows that the maximal H_2 consumption (14.2 μmol/m^2) is observed for the Ag-CeO_2 (co-DP) sample having the minimal surface area (16 m^2 per gram). Taking into account the lowest Ag concentration (Table 1) in this sample, we think that the oxidized silver state in the co-DP sample can play the main role, since the co-DP catalyst shows the lowest AP value due to the formation of the oxidized state of Ag (such as in $AgNO_3$) at the Ce-Ag-O interface. Table 4 shows that the order of catalysts with respect to H_2 consumption per m^2 is Ag-CeO_2 (co-DP) > Ag/CeO_2 (red-imp) > Ag/CeO_2 (imp) in the temperature region of 0–350 °C.

The broad TPR peak in the range of 350–650 °C refers to the reduction of ceria surface. The amount of H_2 consumed in this region correlates with the extent of interaction between the ceria surface and Ag that is a function of the preparation method. All Ag/CeO_2 catalysts exhibit lower H_2 consumption (54–105 μmol/g, Table 3) in comparison with the CeO_2 support (145 μmol/g). The lowest H_2 consumption value was registered for the Ag/CeO_2 (red-imp) catalyst (54 μmol/g or 2.5 μmol/m^2) characterized by the most pronounced interaction between the Ag and CeO_2. High hydrogen consumption value (105 μmol/g and 3.2 μmol/m^2) recorded at 350–750 °C for the Ag/CeO_2 (imp) catalyst suggests the highest amount of Ce (III) (28%) according to the XPS data (Table 2) and a weak Ag–CeO_2 interaction for this catalyst.

Thus, based on the TPR results we can conclude that:

1) the silver species in the Ag/CeO_2 catalysts exist both in metallic and ionic states, and the highest amount of oxidized silver is observed for the Ag/CeO_2 (co-DP) catalyst,
2) H_2 consumption per m^2 in the temperature region of 0–350 °C is increased in the following order: Ag-CeO_2 (co-DP) > Ag/CeO_2 (red-imp) > Ag/CeO_2 (imp)",
3) silver facilitates the low-temperature reduction of surface ceria at 150–250 °C involving the active oxygen species of ceria in the catalytic low-temperature oxidation,
4) the decreased intensity of reduction peaks of surface ceria (350–750 °C) in the Ag/CeO_2 catalysts compared to pure ceria may be used to measure the strength of the Ag–CeO_2 interfacial interaction that increases in the following row: Ag/CeO_2 (imp) ≈ Ag-CeO_2 (co-DP) < Ag/CeO_2 (red-imp) catalysts.

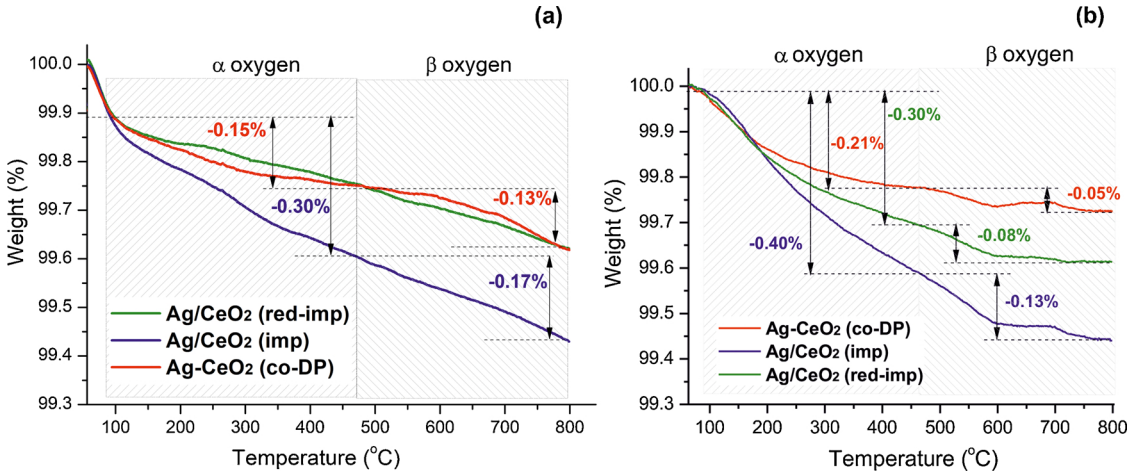

Fig. 7. TGA curves calculated from step 6 (see experimental part) for fresh Ag/CeO_2 (a) and spent Ag/CeO_2 (b) catalysts.

TGA experiments were carried out in order to get further insights into the oxygen vacancies content in the prepared catalysts. Fig. 7a shows the weight (%) curves for the Ag-containing fresh catalysts registered in the range of 25–800 °C under N_2 flow after the pretreatment up to 150 °C under O_2 flow. For all fresh samples, a preliminary weight loss corresponding to 0.1% was observed after heating up to 100 °C likely corresponding to the removal of physically adsorbed oxygen. Then in the range of 100–800 °C, two main regions were detected below and above ~500 °C corresponding to the removal of surface and bulk oxygen species, respectively. According to the literature [100,101], such species are also denoted as α and β oxygen. According to the TPR-H_2 results (see Table 4, H_2 consumption in the range 0–350 °C), the Ag/CeO_2 (imp) catalyst exhibits the most pronounced weight loss (0.3%) likely due to the removal of active oxygen chemisorbed over the Ag species dispersed at the catalyst surface. Accordingly, such catalyst exhibits the highest XPS-derived Ag/Ce ratio (Table 2). Above 500 °C, the desorption of the so-called "β oxygen" associated to "interfacial or bulk" species usually takes place, with the extent of such evolution peaks and the temperature being strongly dependent on the nature of the reducible materials [102]. Confirming again the TPR-H_2 results, above 500 °C the Ag/CeO_2 (imp) catalyst releases the highest amount of oxygen (weight loss of 0.17%) that is likely removed from the surface of ceria at the interface with silver (see Table 3, the temperature range of 350–750 °C). In case of Ag-CeO_2 (co-DP) and Ag/CeO_2 (red-imp), the lower content of surface silver detected by XPS takes into account the lower surface "α oxygen" uptake and release registered during the TGA analysis (weight loss equals to 0.15%). Moreover, both catalysts exhibit higher content of bulk oxygen vacancies with respect to the Ag/CeO_2 (imp) (see Raman data, section 3.3) and, therefore, a lower amount of bulk oxygen can be removed from such samples in the temperature range of ~500 °C, the weight loss equals to 0.13%.

In addition, the TGA experiments were carried out for the spent catalysts (Fig. 7b) after CO oxidation. The TGA curves exhibit similar trends for fresh and spent catalysts. The Ag/CeO_2 (imp) catalyst is characterized by the highest weight loss (0.47% and 0.53% for fresh and spent samples, respectively) confirming that this sample releases the highest amount of oxygen species. The weight loss for fresh and spent Ag-CeO_2 (co-DP) is equal to 0.28% and 0.26%, respectively, while for Ag/CeO_2 (red-imp) the oxygen release corresponds to 0.28% and 0.38%, respectively for the fresh and spent sample. A comparison of the overall weight loss registered at 800 °C shows that an increased amount of oxygen is released by Ag/CeO_2 (imp) and the spent Ag/CeO_2 (red-imp) catalysts as compared to the corresponding fresh samples, while comparable values were obtained for the Ag-CeO_2 (co-DP). However, a perusal of each TGA curve reveals that the respective amounts of α and β oxygen is removed for each fresh and spent catalyst change. Indeed, for all samples, the amount of the removed α oxygen species increased after CO oxidation (higher amount of surface oxygen vacancies), while less β oxygen is removed after the reaction. Such a decrease in the amount of β oxygen is particularly indicative for the spent Ag-CeO_2 (co-DP) (the weight loss is 0.05%). The observed trend is connected with the participation of mainly the lattice ceria oxygen in CO oxidation. This is consistent with the Raman data.

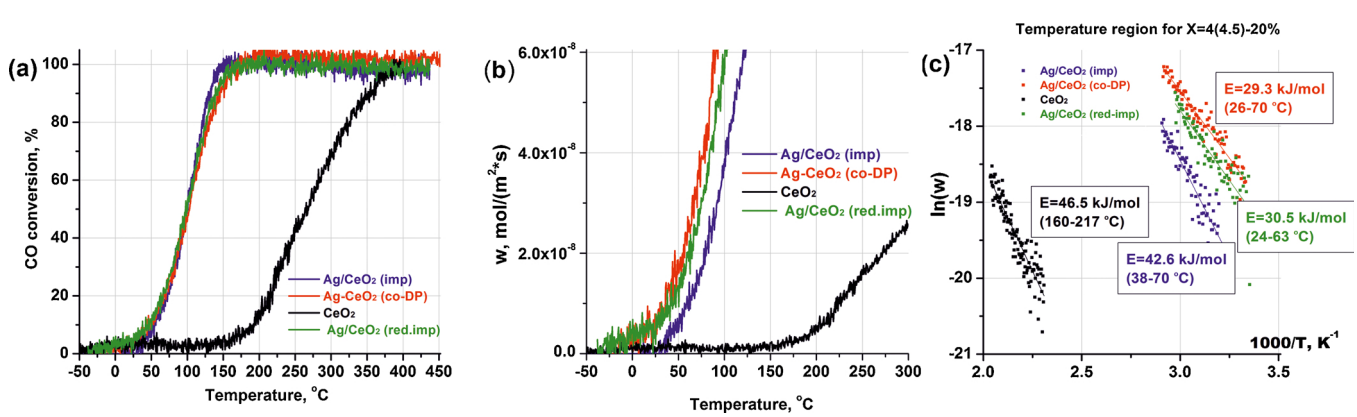

Fig. 8. Temperature dependences of CO conversion (a), temperature dependence of reaction rate (b) and Arrhenius plot for the apparent activation energy (c) after 2nd cycle.

Table 5
Catalytic properties of Ag/CeO_2 catalysts in the CO oxidation reaction.

	E_a, kJ/mol	Conditions	$T_{50\%}$, °C	Rate at 50 °C, CO molecules (m^2 s)	Ref.
CeO_2	54.6 (1st cycle)	0.5 % CO, 4.4 % O_2	290	4.2×10^{-10}	this work
	46.5 (2nd cycle)	300 ml/min, 0.45 g	265	1.3×10^{-9}	
Ag/CeO_2 (imp)	45.9 (1st cycle)	0.5 % CO, 4.4 % O_2	99	1.5×10^{-9}	this work
	42.6 (2nd cycle)	300 ml/min, 0.45 g	97	6.7×10^{-9}	
Ag-CeO_2 (co-DP)	44.8 (1st cycle)	0.5 % CO, 4.4 % O_2	106	5.6×10^{-9}	this work
	29.3 (2nd cycle)	300 ml/min, 0.45 g	101	1.7×10^{-8}	
Ag/CeO_2 (red-imp)	28.9 (1st cycle)	0.5 % CO, 4.4 % O_2	103	1.2×10^{-8}	this work
	30.5 (2nd cycle)	300 ml/min, 0.45 g	98	1.3×10^{-8}	
Ag/CeO_2-600 (4.65 wt.% Ag)	32.8 (1st cycle)	0.2% CO, 1.0 % O_2	150	–	[78]
	46.3 (2nd cycle)	240 000 h^{-1}	~210	–	
		1000 ml/min, 0.2 g			
Ag/CeO_2 (4.65 wt.% Ag)	75.7 (1st cycle)	0.2% CO, 1.0 % O_2	~230	–	[78]
	44.9 (2nd cycle)	240 000 h^{-1}	140	–	
		1000 ml/min, 0.2 g			
CeO_2-Ag (10 wt.% Ag)	–	1 % CO, 10 % O_2,	132	–	[103]
		60 000 mL/(g·h),			
	–	100 ml/min, 0.1 g	–	–	
Ag/CeO_2	–	1% CO, 1.0 % O_2	~160	–	[74]
(5 wt.% Ag)	–	36 000 mL/(g·h), 0.1 g	–	–	
Ag/CeO_2	–	1000 ppm CO in air,	~220	–	[86]
(6 wt.% Ag)	–	60 000 mL/(g·h),	–	–	
		50 ml/min, 0.05 g			
Ag–CeO_2-A (Ag/Ce = 1.14 mol. ratio)	–	1% CO in air,	~85	3.2×10^{-8}	[59]
	–	12 000 mL/(g·h),	~90	4.1×10^{-8}	
		20 ml/min, 0.1 g			
Ag/CeO_2-HP (8 wt.% Ag)	–	1 % CO, 20 % O_2	44	8.6×10^{-9}	[47]
	–	13 000 h^{-1}		– –	
		30 ml/min, 0.2 g			

3.5. Catalytic performance in CO oxidation

The catalytic test of the prepared samples was carried out in CO oxidation reaction. Fig. 8 shows the temperature dependences of CO conversion (a), the CO oxidation rate (b), and the Arrhenius plot for the apparent activation energy for CO oxidation rate (c) after 2nd cycle. The CeO_2 support is active in CO oxidation at temperatures above 150 °C, and a total conversion of CO is achieved at ~400 °C. The addition of Ag into ceria significantly improves the catalytic performance in CO oxidation. CO conversion begins at room temperature for all Ag-containing catalysts, the 50% CO conversion is achieved at 100 °C and total CO conversion is achieved below 170 °C.

To compare the catalytic activity of CeO_2, Ag/CeO_2 (imp), Ag-CeO_2 (co-DP) and Ag/CeO_2 (red-imp) catalysts, the reaction rates in terms of CO molecules converted at 50 °C per second and per m^2 were calculated during the first and second cycles and are listed in Table 5 along with the activation energies. For comparison reasons, Table 5 reports some kinetic data from the literature and the corresponding experimental conditions used.

After the second catalytic cycle, an increase in the CO oxidation rate and a decrease of E_a values occur for CeO_2 and all Ag supported catalysts (see Table 5 and Fig. 8b and 8c). Among silver catalysts, Ag-CeO_2 (co-DP) and Ag/CeO_2 (red-imp) are more active than Ag/CeO_2 (imp). The E_a values calculated during the second cycle are equal to 29.3 and 30.5 kJ/mol, for the first two samples, while the value for the impregnated one is 42.6 kJ/mol. Furthermore, the latter catalyst shows the reaction rate and E_a values (42.6 vs 46.5 kJ/mol during the second cycle) close to those of pure CeO_2.

The above-mentioned data support the occurrence of the MSI for two samples, Ag-CeO_2 (co-DP) and Ag/CeO_2 (red-imp), and the positive effect of the second cycle that makes such an interaction stronger. Conversely, silver particles and ceria weakly interact in the case of Ag/CeO_2 (imp) not generating oxygen vacancies as active sites for CO oxidation. Table 5 summarizes the catalytic data on Ag/CeO_2 catalysts from literature. Kibis et al. [78] studied the CO oxidation over Ag/CeO_2 catalyst prepared by pulsed laser ablation in liquids (PLA) and found relatively low values of activation energies. Besides, during the second cycle, the activity changes significantly depending on the calcination temperature that strongly affects the MSI: The activity of the as-prepared Ag/CeO_2 catalyst increases that is consistent with our results, while the activity of the Ag/CeO_2-600 (calcined at 600 °C) dramatically decreases which was attributed to the silver redistribution on the ceria surface and, therefore, to a decreased MSI.

The CO oxidation data support the occurrence of MSI for Ag-CeO_2 (co-DP) and Ag/CeO_2 (red-imp) that becomes stronger upon the 2nd cycle, in agreement with the Raman and TGA characterization results on fresh and used catalysts. The comparison of the catalytic data with those registered over Ag/CeO_2 catalysts in Refs. [47,59] (see Table 5) is difficult because of the high Ag content in the catalyst composition and different experimental conditions, such as low flow rate (12 000 mL/(g·h) and 13 000 h^{-1}, respectively), 99% air (that can overheat the catalytic bed).

3.6. Catalytic performance in soot oxidation

To study the catalytic activity of the samples in soot oxidation the simultaneous thermal analysis (STA-TGA) was used. Soot oxidation has been carried out using air in a temperature range of 230–640 °C and under tight contact conditions. Fig. 9 shows the TG and DTG curves for a simulation of diesel soot oxidation for the CeO_2 support and Ag/CeO_2 catalysts. Non-catalytic soot oxidation occurs at 550–700 °C. The presence of CeO_2 shifts the reaction temperature to 400–650 °C. Soot oxidation over Ag/CeO_2 catalysts is observed in a temperature range of 230–640 °C with T_{max} = 390 °C for Ag/CeO_2 (red-imp) and T_{max} = 415 °C for Ag-CeO_2 (co-DP), respectively. Over the Ag/CeO_2 (imp) the reaction occurs between 300 and 680 °C with T_{max} = 460 °C (Fig. 9).

4. Discussion

Results of characterization of the catalysts evidence the interfacial interaction between the Ag and CeO_2. The strongest interfacial Ag–CeO_2 interaction on Ag/CeO_2 catalysts is observed for the samples prepared by co-deposition and impregnation of the prereduced CeO_2. The enhanced interfacial interaction is mainly a result of the redox

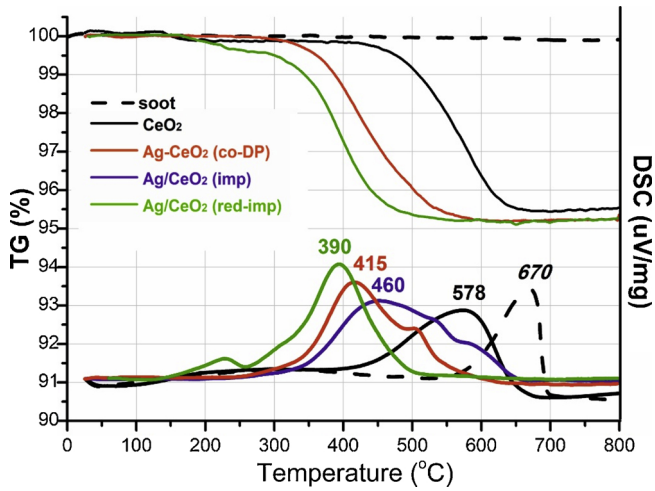

Fig. 9. TGA and DSC curves for soot oxidation over CeO_2 support and Ag/CeO_2 catalysts.

reaction between Ce^{3+} and Ag^{+} that occurs during the catalyst preparation. According to N_2 adsorption/desorption, these catalysts are characterized by a significant decrease in the pore volume and S_{BET} in comparison with those of CeO_2 and Ag/CeO_2 (imp). This may be caused by the interaction of silver precursors with the support during the synthesis accompanied by a reconstruction of the primary ceria particles and their growth (an increased particle size of CeO_2 according to XRD results). The epitaxial growth of silver on the surface of ceria due to the strong metal-support binding is observed by TEM HR for both Ag-CeO_2 (co-DP) and Ag/CeO_2 (red-imp) catalysts. Therefore, the textural features of the catalysts should affect the catalytic properties. The XRD patterns confirm the enhanced Ag–CeO_2 interaction for the Ag-CeO_2 (co-DP) and Ag/CeO_2 (red-imp) catalysts with a shift to lower angle from ~28.59° to 28.48° 2θ. The increase in the cell parameter of ceria in the Ag-CeO_2 (co-DP) calculated based on the XRD data indicates an increase in the number of oxygen vacancies in the CeO_2 structure. To sum up, all these results indicate the incorporation of silver into the structure of ceria yielding the Ag–CeO_2 interface with an enhanced interfacial interaction. The XPS data show the additional salt-like state of silver for the Ag-CeO_2 (co-DP) catalyst that confirms the presence of Ag^{+} species in the CeO_2 structure.

The introduction of Ag on CeO_2 significantly enhances the reducibility of the surface capping oxygen of CeO_2 that is shown by TPR. The new O^{-} species for Ag/CeO_2 catalysts make the Ag/CeO_2 catalysts distinctive in comparison with Ag/SiO_2 [104], Ag/TiO_2 [105] and other supported silver catalysts. The maximal amounts of surface and bulk oxygen vacancies are detected by Raman spectroscopy for Ag-CeO_2 (co-DP) and Ag/CeO_2 (red-imp) catalysts, respectively. Thus, we conclude that the increased amount of oxygen vacancies for Ag-CeO_2 (co-DP) and Ag/CeO_2 (red-imp) catalysts is a result of the strengthening of the metal-support interactions.

Higher activity of the Ag-CeO_2 (co-DP) and Ag/CeO_2 (red-imp) catalysts in CO oxidation may be attributed to the enhanced Ag–CeO_2 interfacial interaction in these catalysts in comparison with Ag/CeO_2 (imp) catalyst. The enhanced Ag-CeO_2 interfacial interaction leads to both charge redistribution between the Ag and CeO_2 and increase of the amount of oxygen vacancies in the ceria support. This leads to higher reaction ability of Ag/CeO_2 catalysts towards CO and molecular oxygen. The possible cooperation of the silver and ceria species on the Ag–CeO_2 in CO oxidation also should be taken into account. The enhanced and extended interfacial boundary in the Ag-CeO_2 (co-DP) and Ag/CeO_2 (red-imp) catalysts is favorable for low-temperature CO oxidation.

Thus, the reaction mechanism is close to the one for the CO oxidation over the pure ceria and is practically independent on the deposited silver. As shown in Ref. [106], the lattice oxygen mainly participates in the oxidation of CO over CeO_2 and partly over the reduced CeO_x:

$$CO + * \rightarrow CO_{ads}$$

$$CO_{ads} + O^{2-}_{surf} \rightarrow \square^{2-} + CO_2,$$

where $O_{surf}{}^{2-}$ represents a lattice oxygen. In the presence of CO molecules, the ceria reduction occurs at an adsorption site (*), which is an oxygen ion at the surface of the NPs. After the reaction, the product comprising CO_2 molecule desorbs from the surface leaving a charged oxygen vacancy $\square^{2-}$.

Reoxidation of the formed vacancies can occur at their interacting with the gas-phase oxygen and due to diffusion of the atoms from the bulk and surface. Moreover, the rate of the diffusion process depends on the temperature and the presence of bulk vacancies [107]. The higher is the amount of vacancies accumulated in the bulk, the lower is the contribution of the O^{-} diffusion to re-oxidation processes in the range of $T < 200$. In our case, for the Ag/CeO_2 (imp), such a reoxidation mechanism will prevail due to the minimal content of the bulk vacancies. The reason for this is connected with the absence of the enhanced interaction between the Ag and CeO_2 NPs for the Ag/CeO_2 (imp) catalyst. For the Ag/CeO_2 (red-imp) and Ag-CeO_2 (co-DP) samples, the obtained values of the apparent E_a are close to each other (30 and 29 kJ/mol, respectively). Such a decrease in the values of the apparent E_a is associated with a partial transfer of the electron density during the formation of the epitaxially connected Ag clusters on the ceria surface (TEM results). The formation of the aggregate structures between the Ag and CeO_2 changes the CO oxidation mechanism, and the main changes are probably associated with the activation of the gas-phase oxygen yielding the surface adsorbed species that are able to participate in CO oxidation. The presence of the surface defects in the Ag-CeO_2 (co-DP) sample (Raman data) contributes to the formation of a large amount of O_{ads} in comparison with the Ag/CeO_2 (red-imp) sample. The presence of a large concentration of bulk vacancies significantly decreases the contribution of the diffusion mechanism and contributes to an increase in the fraction of the reaction with the formation of O_{ads}.

The mechanism of soot oxidation is currently under discussion [15]. The adsorbed active oxygen species play a key role in all oxidative processes that occur on the surface of Ag/CeO_2 catalysts. The reoxidation of the surface by the adsorbed oxygen species occurs independently on the type of the carrier gas according to the following sequential scheme [88]:

$$O^{-}_{2\,ads} \rightarrow O^{2-}_{2\,ads} \rightarrow 2O^{-}_{ads} \rightarrow 2O^{2-}_{lattice}$$

According to this scheme, the surface peroxide species are more thermally stable than superoxides, and the peroxides are able to convert into the lattice oxygen.

The role of both oxygen vacancies and adsorbed oxygen in the oxidation of soot particle and realization of the Mars-van Krevelen mechanism are under close attention. Different oxygen species ($O_n{}^{x-}$) in the CeO_2 and Ag/CeO_2 catalysts, which are active in soot oxidation, are described in the literature:

- superoxide adsorbed $O_2{}^{-}$ species, which is formed due to electron transfer from the metallic Ag NPs [108] or/and as a result of the interaction of surface vacancies ($V_{O\text{-}s}$) of CeO_2 with the gas-phase oxygen [109],
- adsorbed oxygen (O_{ads}) species on the interfacial boundaries between the Ag NPs and ceria,
- oxygen (O^{2-}) species in the crystalline lattice on the CeO_2 surface [53].

The activity of Ag/CeO_2 catalysts in soot oxidation is generally attributed to the features of ceria, while the role of silver in activation of

oxygen is not clear [43]. Corro et al. [108] studied the electronic state of silver in Ag/SiO_2 and Ag/ZnO catalysts and its effect on the oxidation of diesel particulate matter. It was established that the 3% Ag/SiO_2 catalyst was characterized by the highest activity in oxidation process due to a high amount of metallic Ag^0 (the particle size was 2–5 nm) at the surface, which was able to form high amounts of O_2^- species. Thus, both CeO_2 and silver are able to participate in the formation of the adsorbed O_2^- superoxide species on the surface of Ag/CeO_2 catalysts. However, it is noteworthy that several Ag-containing species should co-exist on the Ag/CeO_2 and provide a tight contact with the support.

Wu et al. [109] studied the influence of the surface ($V_{O\text{-}s}$) and bulk ($V_{O\text{-}b}$) oxygen vacancies on the soot oxidation over CeO_2 and 5% Ag/CeO_2 prepared by the wet impregnation method from the water solution of Ag NO_3. The authors concluded that the addition of the Ag decrease the amount of surface ($V_{O\text{-}s}$) vacancies with a simultaneous increase of the bulk oxygen vacancies. Thus, the role of silver was connected with the redistribution between the surface and bulk oxygen vacancies. Recently, Wang et al. [110] reported that the activity growth of CeO_2 nanorods and Ag/CeO_2 in soot oxidation was connected with the increased amount of vacancies.

In the present work, the activity of the catalysts in soot oxidation increased in the following row: CeO_2 < Ag/CeO_2 (imp) < Ag-CeO_2 (co-DP) < Ag/CeO_2 (red-imp.) (Fig. 9). The amount of oxygen vacancies detected in the catalysts (see Raman results, Fig. 5, Table 3) increases in the same order. Thus, it can be surmised that the enhanced metal-support interaction also facilitates soot oxidation activity.

It was found for the Ag/CeO_2 (imp) catalyst that the addition of silver to ceria yields weakly bond adsorbed oxygen species over both silver and ceria detected by XPS (BE = 532.2 eV, attributed to the surface-chemisorbed oxygen species or OH groups), TG (Fig. 7) and TPR-H_2 (Fig. 6). However, no significant changes in the structure of ceria occurred for the Ag/CeO_2 (imp) catalyst (XRD results), and a small amount of oxygen vacancies was detected by Raman. The activity growth of the Ag/CeO_2 (imp) in CO and soot oxidation in comparison with the pure ceria is mainly attributed to the small size of silver NPs and a partial activation of the surface oxygen of ceria in the presence of silver (TPR-H_2 results, Fig. 6). With that, TPR-H_2 results show that the peak from 350 to 650 °C attributed to the reduction of surface ceria is relatively intensive indicating that a part of ceria NPs are not covered by silver. This explains the double-peak oxidation of soot over this catalyst (Fig. 9), where the first peak may be attributed to soot oxidation over ceria NPs with the participation of silver, and the second peak is a result of soot combustion over silver-free ceria particles.

Different silver particles are observed in the Ag-CeO_2 (co-DP) catalyst by TEM: weakly bound Ag clusters (Fig. S1), epitaxially bound Ag particles over ceria surface (Fig.3, c–d) and large well crystalline silver particles with a size of 5–8 nm (Fig. S2). The formation of different silver species in this catalyst is connected with the competitive reactions during the co-deposition: precipitation of $Ce(OH)_3$ and [AgOH], redox reaction between Ce^{3+} and Ag^+. It is noteworthy that according to XPS data, the O1s peak is shifted up to 529.7 eV that may be associated with the integral signal from both ionic oxygen species weakly bound with Ag surface and the oxygen ions in the oxygen-deficient regions within the CeO_2 lattice (the bulk oxygen vacancies). The results of Raman studies indicate the co-existence of the surface and bulk oxygen vacancies for Ag-CeO_2 (co-DP) catalyst (Fig. 5). Thus, different oxygen vacancies can be located on different particles. In general, the Ag-CeO_2 (co-DP) catalyst is more active in comparison with the Ag/CeO_2 (imp) catalyst in both CO and soot oxidation that may be a result of the enhanced Ag-CeO_2 interfacial interaction in this catalyst.

In the case of Ag/CeO_2 (red-imp) catalyst, the small metal Ag^0 clusters (with sizes close to 1 nm) uniformly distributed on the ceria surface were observed by TEM HR. The metal state of Ag clusters is a result of the redox reaction between the Ag^+ ions in the impregnating solution and the Ce^{3+} species on the surface of the prereduced CeO_2. The epitaxial growth of silver cluster on the ceria surface was observed by TEM HR (Fig. 3e) and indicated the strengthening of the Ag/CeO_2 interaction in this catalyst.

According to the Raman data, the surface oxygen vacancies are not observed for Ag/CeO_2 (red-imp) catalyst, while the amount of bulk oxygen vacancies is maximal. In [53], the authors argue that the content of the bulk oxygen vacancies is more important in real soot oxidation over ceria-based catalysts. In the present work, the Ag/CeO_2 (red-imp) catalyst has the highest activity in soot oxidation that may be connected with both high amount of bulk oxygen vacancies and a co-operation of strongly bound small silver clusters with ceria.

Thus, the enhanced interfacial interaction in the Ag/CeO_2 catalysts allows creating the surface with the highest reaction ability able to generate mainly the surface peroxide oxygen species taking part in the soot oxidation at low temperatures. The control of the Ag–CeO_2 interfacial interaction plays a crucial role in the development of highly effective silver-containing catalysts for oxidation reactions. The redox reaction between Ce^{3+} and Ag^+ during the co-deposition and red-impregnation was demonstrated to be an effective way to enhance the interfacial interaction and improve the catalytic properties. Thus, the enhanced Ag–CeO_2 interaction increases the reducibility and content of oxygen vacancies of ceria and plays a key role in enhancing the catalytic performance of Ag/CeO_2 catalysts in low-temperature CO oxidation and soot combustion. The strong metal-support bonding in the Ag/CeO_2 catalysts was detected as the epitaxial growth of silver NPs on the surface of ceria (TEM HR), the distortion of CeO_2 lattice (XRD) and an increased amount of oxygen vacancies (Raman). The enhanced interfacial interaction leads to increased reducibility and a cooperation of oxidized species of both silver and ceria in CO and soot oxidation. The enhanced Ag–CeO_2 interfacial interaction facilitates the enhancement of the rate of reoxidation of active species that according to Mars–van Krevelen mechanism provides the oxidation of CO and soot.

5. Conclusions

In the present work the Ag/CeO_2 catalysts have been synthesized by three different methods comprising the impregnation, co-deposition precipitation and impregnation of the prereduced ceria. For the first time, it was shown that the redox reaction between silver (I) and cerium (III) during the component co-precipitation (Ag/CeO_2 (co-DP)) or impregnation stages of the pre-reduced ceria (Ag/CeO_2 (red-imp)) plays the key role in the formation of Ag–CeO_2 interface with the enhanced interaction.

A complex of complementary experimental techniques was used to confirm the presence of strong interfacial interaction between Ag and CeO_2 support. For the first time, a complex of structural changes (XRD, TEM HR), changes of chemical states of both silver and cerium (XPS, Raman), reaction ability (TPR, TGA) and catalytic properties in low-temperature CO oxidation and middle-temperature soot combustion was demonstrated. It was clearly shown that the correlation between the catalytic properties and the metal-support interaction occurs in Ag/CeO_2 catalysts. The enhancement of the MSI in following order: Ag/CeO_2 (imp) < Ag-CeO_2 (co-DP) ≤ Ag/CeO_2 (red-imp) correlates with the increase of the catalytic activity for both CO and soot oxidation due to the increased amount of oxygen vacancies in the Ag/CeO_2 catalysts.

Thus, the control of the metal–support interaction is a key factor for designing of highly effective inexpensive catalysts without Pd, Pt, Ru for environmental applications.

Declaration of Competing Interest

The authors declare that they have no known competing financial interests or personal relationships that could have appeared to influence the work reported in this paper.

Acknowledgements

The authors greatly acknowledge the Center of the instruments and equipment "High-tech and nano-analyst of Novosibirsk State University" for TEM HR studies, Valery A. Svetlichnyi (Tomsk State University, Russia) for Raman studies. The authors also thank Dr. Mikhail A. Salaev (Tomsk State University) for language review.

This work was supported by Russian Science Foundation (Grant № 18-73-10109) and "The Tomsk State University competitiveness improvement programme" (Project № 8.2.03.2018).

Appendix A. Supplementary data

Supplementary material related to this article can be found, in the online version, at doi:https://doi.org/10.1016/j.apcatb.2019.118148.

References

[1] E. Aneggi, C. de Leitenburg, A. Trovarelli, Ceria-based formulations for catalysts for diesel soot combustion, second ed., in: A. Trovarelli, P. Fornasiero (Eds.), Catalysis by Ceria and Related Materials, vol. 12, Imperial College Press, London, 2013, pp. 565–621.

[2] J.A. Rodriguez, D.C. Grinter, Z. Liu, R.M. Palomino, S.D. Senanayake, Ceria-based model catalysts: fundamental studies on the importance of the metal–ceria interface in CO oxidation, the water–gas shift, CO_2 hydrogenation, and methane and alcohol reforming, Chem. Soc. Rev. 46 (2017) 1824–1841, https://doi.org/10.1039/C6CS00863A.

[3] M. Skaf, S. Aouad, S. Hany, R. Cousin, E. Abi-Aadand, A. Aboukais, Physicochemical characterization and catalytic performance of 10% Ag/CeO_2 catalysts prepared by impregnation and deposition–precipitation, J. Catal. 320 (2014) 137–146, https://doi.org/10.1016/j.jcat.2014.10.006.

[4] S. Scirè, P.M. Riccobene, C. Crisafulli, Ceria supported group IB metal catalysts for the combustion of volatile organic compounds and the preferential oxidation of CO, Appl. Catal. B Environ. 101 (2010) 109–117, https://doi.org/10.1016/j.apcatb.2010.09.013.

[5] J. Lin, X. Wang, T. Zhang, Recent progress in CO oxidation over Pt-group-metal catalysts at low temperatures, Chinese J. Catal. 37 (2016) 1805–1813, https://doi.org/10.1016/S1872-2067(16)62513-5.

[6] M.S. Chen, Y. Cai, Z. Yan, K.K. Gath, S. Axnanda, D. Wayne Goodman, Highly active surfaces for CO oxidation on Rh, Pd, and Pt, Surf. Sci. 601 (2007) 5326–5331, https://doi.org/10.1016/j.susc.2007.08.019.

[7] T.-S. Nguyen, F. Morfin, M. Aouine, F. Bosselet, J.-L. Rousset, L. Piccolo, Trends in the CO oxidation and PROX performances of the platinum-group metals supported on ceria, Catal. Today 253 (2015) 106–114, https://doi.org/10.1016/j.cattod.2014.12.038.

[8] J. Xu, J. Zhang, H. Peng, X. Xu, W. Liu, Z. Wang, N. Zhang, X. Wang, Ag supported on mesostructured SiO_2 with different morphologies for CO oxidation: on the inherent factors influencing the activity of Ag catalysts, Microporous Mesoporous Mater. 242 (2017) 90–98, https://doi.org/10.1016/j.micromeso.2017.01.016.

[9] L. Yu, Y. Shi, Z. Zhao, H. Yin, Y. Wei, J. Liu, W. Kang, T. Jiang, A. Wang, Ultrasmall silver nanoparticles supported on silica and their catalytic performances for carbon monoxide oxidation, Catal. Commun. 12 (2011) 616–620, https://doi.org/10.1016/j.catcom.2010.12.012.

[10] G.V. Mamontov, A.S. Gorbunova, E.V. Vyshegorodtseva, V.I. Zaikovskii, O.V. Vodyankina, Selective oxidation of CO in the presence of propylene over Ag/MCM-41 catalyst, Catal. Today (2018), https://doi.org/10.1016/j.cattod.2018.05.015 In Press.

[11] V.V. Dutov, G.V. Mamontov, V.I. Zaikovskii, L.F. Liotta, O.V. Vodyankina, Low-temperature CO oxidation over Ag/SiO_2 catalysts: effect of OH/Ag ratio, Appl. Catal. B Environ. 221 (2018) 598–609, https://doi.org/10.1016/j.apcatb.2017.09.051.

[12] E. Kolobova, A. Pestryakov, G. Mamontov, Y. Kotolevich, N. Bogdanchikova, M. Farias, A. Vosmerikov, L. Vosmerikova, V. Cortes Corberan, Low-temperature CO oxidation on Ag/ZSM-5 catalysts: influence of Si/Al ratio and redox pretreatments on formation of silver active sites, Fuel 188 (2017) 121–131, https://doi.org/10.1016/j.fuel.2016.10.037.

[13] K. Villani, R. Brosius, J.A. Martens, Catalytic carbon oxidation over Ag/Al_2O_3, J. Catal. 236 (2005) 172–175, https://doi.org/10.1016/j.jcat.2005.09.018.

[14] P. Li, X. Chen, Y. Li, J.W. Schwank, A review on oxygen storage capacity of CeO_2-based materials: Influence factors, measurement techniques, and applications in reactions related to catalytic automotive emissions control, Catal. Today (2018), https://doi.org/10.1016/j.cattod.2018.05.059 In Press.

[15] M.V. Grabchenko, N.N. Mikheeva, G.V. Mamontov, M.A. Salaev, L.F. Liotta, O.V. Vodyankina, Ag/CeO_2 composites for catalytic abatement of CO, soot and VOCs, Catalysts 8 (2018) 285, https://doi.org/10.3390/catal8070285.

[16] S. Liu, X. Wu, D. Weng, R. Ran, Ceria-based catalysts for soot oxidation: a review, J. Rare Earth 33 (2015) 567–590, https://doi.org/10.1016/S1002-0721(14)60457-9.

[17] R.V. Gulyaev, E.M. Slavinskaya, S.A. Novopashin, D.V. Smovzh, A.V. Zaikovskii, D.Yu. Osadchii, O.A. Bulavchenko, S.V. Korenev, A.I. Boronin, Highly active PdCeOx composite catalysts for low-temperature CO oxidation, prepared by plasma-arc synthesis, Appl. Catal. B Environ. 147 (2014) 132–143, https://doi.org/10.1016/j.apcatb.2013.08.043.

[18] E.M. Slavinskaya, R.V. Gulyaev, A.V. Zadesenets, O.A. Stonkus, V.I. Zaikovskii, Yu.V. Shubin, S.V. Korenev, A.I. Boronin, Low-temperature CO oxidation by Pd/CeO_2 catalysts synthesized using the coprecipitation method, Appl. Catal. B Environ. 166–167 (2015) 91–103, https://doi.org/10.1016/j.apcatb.2014.11.015.

[19] G. Si, J. Yua, X. Xiao, X. Guo, H. Huang, D. Mao, G. Lu, Boundary role of Nano-Pd catalyst supported on ceria and the approach of promoting the boundary effect, J. Mol. Catal. 444 (2018) 1–9, https://doi.org/10.1016/j.mcat.2017.10.025.

[20] A.I. Stadnichenko, V.V. Muravev, S.V. Koscheev, V.I. Zaikovskii, H.A. Aleksandrov, K.M. Neymand, A.I. Boronin, Study of active surface centers of Pt/CeO_2 catalysts prepared using radio-frequency plasma sputtering technique, Surf. Sci. 679 (2019) 273–283, https://doi.org/10.1016/j.susc.2018.10.002.

[21] F. Morfin, T.S. Nguyen, J.L. Rousset, L. Piccolo, Synergy between hydrogen and ceria in Pt-catalyzed CO oxidation: An investigation on Pt–CeO_2catalysts synthesized by solution combustion, Appl. Catal. B Environ. 197 (2016) 2–13, https://doi.org/10.1016/j.apcatb.2016.01.056.

[22] J. Lee, Y. Ryou, J. Kim, X. Chan, T.J. Kim, D.H. Kim, Influence of the defect concentration of Ceria on the Pt dispersion and the CO oxidation activity of Pt/CeO_2, Phys. Chem. C 122 (2018) 4972–4983, https://doi.org/10.1021/acs.jpcc.8b00254.

[23] A. Satsuma, M. Yanagihara, J. Ohyama, K. Shimizu, Oxidation of CO over Ru/Ceria prepared by self-dispersion of Ru metal powder into nano-sized particle, Catal. Today 201 (2013) 62–67, https://doi.org/10.1016/j.cattod.2012.03.048.

[24] E. Vargas, A. Simakov, R. Rangel, F. Castillon, Houston, Texas20th North American Catalysis Meeting2007, 20th North American Catalysis Meeting (2007).

[25] A.A. El-Moemen, A.M. Abdel-Mageed, J. Bansmann, M. Parlinska-Wojtan, R.J. Behm, G. Kucerová, Deactivation of Au/CeO_2 catalysts during CO oxidation: influence of pretreatment and reaction conditions, J. Catal. 341 (2016) 160–179, https://doi.org/10.1016/j.jcat.2016.07.005.

[26] R. Zhang, K. Lu, L. Zong, S. Tong, X. Wang, G. Feng, Gold supported on ceria nanotubes for CO oxidation, Appl. Surf. Sci. 416 (2017) 183–190, https://doi.org/10.1016/j.apsusc.2017.04.158.

[27] R. Zhang, K. Lu, L. Zong, S. Tong, X. Wang, J. Zhou, Z.-H. Lu, G. Feng, Control synthesis of CeO_2 nanomaterials supported gold for catalytic oxidation of carbon monoxide, J. Mol. Catal. 442 (2017) 173–180, https://doi.org/10.1016/j.mcat.2017.09.024.

[28] S. Aouad, E. Abi-Aad, A. Aboukais, Simultaneous oxidation of carbon black and volatile organic compounds over Ru/CeO_2 catalysts, Appl. Catal. B Environ. 88 (2009) 249–256, https://doi.org/10.1016/j.apcatb.2008.10.002.

[29] L.F. Nascimento, R.F. Martins, O.A. Serra, Catalytic combustion of soot over Ru-doped mixed oxides catalysts, J. Rare Earths 32 (7) (2014) 610–620, https://doi.org/10.1016/S1002-0721(14)60116-2.

[30] M. Kurnatowska, L. Kepinski, Structure and thermal stability of nanocrystalline $Ce_{1-x}Rh_xO_{2-y}$ in reducing and oxidizing atmosphere, Mater. Res. Bull. 48 (2013) 852–862, https://doi.org/10.1016/j.materresbull.2012.11.076.

[31] K. Li, X. Wang, Z. Zhou, X. Wu, D. Weng, Oxygen storage capacity of Pt-, Pd-, Rh/CeO_2 -based oxide catalyst, J. Rare Earths 25 (2007) 6–10, https://doi.org/10.1016/S1002-0721(07)60034-9.

[32] E. Aneggi, D. Wiater, C. de Leitenburg, J. Llorca, A. Trovarelli, Shape-dependent activity of Ceria in soot combustion, ACS Catal. 4 (2014) 172–181, https://doi.org/10.1021/cs400850r.

[33] A. Bueno-Lopez, Diesel soot combustion ceria catalysts, Appl. Catal. B Environ. 146 (2014) 1–11, https://doi.org/10.1016/j.apcatb.2013.02.033.

[34] J. Liu, Advanced Electron microscopy of metal–Support interactions in supported metal catalysts, ChemCatChem 3 (2011) 934–948, https://doi.org/10.1002/cctc.201100090.

[35] C.-J. Pan, M.-C. Tsai, W.-N. Su, J. Rick, N.G. Akalework, A.K. Agegnehu, S.-Y. Cheng, B.-J. Hwang, Tuning/exploiting strong metal-support interaction (SMSI) in heterogeneous catalysis, J. Taiwan Inst. Chem. E 74 (2017) 154–186, https://doi.org/10.1016/j.jtice.2017.02.012.

[36] I. Ro, J. Resasco, P. Christopher, Approaches for understanding and controlling interfacial effects in oxide-supported metal catalysts, ACS Catal. 8 (8) (2018) 7368–7387, https://doi.org/10.1021/acscatal.8b02071.

[37] Q. Fu, T. Wagner, Interaction of nanostructured metal overlayers with oxide surfaces, Surf. Sci. Rep. 62 (2007) 431–498, https://doi.org/10.1016/j.surfrep.2007.07.001.

[38] H.E. Michaelson, The work function of the elements and its periodicity, J. Appl. Phys. 48 (1977) 4729–4733, https://doi.org/10.1063/1.323539.

[39] T. Komaya, A.T. Bell, Z. Wengsieh, R. Gronsky, F. Engelke, T.S. King, M. Pruski, Effects of dispersion and metal-metal oxide interactions on Fischer-Tropsch synthesis over Ru/TiO_2 and TiO_2-promoted Ru/SiO_2, J. Catal. 150 (1994) 400–406, https://doi.org/10.1006/jcat.1994.1358.

[40] D. Li, N. Ichikuni, S. Shimazu, T. Uematsu, Hydrogenation of CO_2 over sprayed Ru/TiO_2 fine particles and strong metal–support interaction, Appl. Catal. A General 180 (1999) 227–235, https://doi.org/10.1016/S0926-860X(98)00335-4.

[41] K.H. Meiwes-Broer, Work functions of metal clusters, Hyperfine Interact. 89 (1994) 263–269.

[42] S. Liang, C. Hao, Y. Shi, The power of single-atom catalysis, ChemCatChem 7 (2015) 2559–2567, https://doi.org/10.1002/cctc.201500363.

[43] J.A. Farmer, C.T. Campbell, Ceria maintains smaller metal catalyst particles by strong metal-support bonding, Science 329 (2010) 933–936, https://doi.org/10.1126/science.1191778.

[44] N. Acerbi, S.C. Tsang, S. Golunski, P. Collier, A practical demonstration of electronic promotion in the reduction of ceria coated PGM catalysts, Chem. Commun.

(2008) 1578–1580, https://doi.org/10.1039/B718956G.
[45] X. Qian, Y. Kuwahara, K. Mori, H. Yamashita, Silver nanoparticles supported on CeO_2/SBA-15 by microwave irradiation possess metal–Support interactions and enhanced catalytic activity, Chem. Eur. J. 20 (2014) 15746–15752, https://doi.org/10.1002/chem.201404307.
[46] S. Chang, M. Li, Q. Hua, L. Zhang, Y. Ma, B. Ye, W. Huang, Shape-dependent interplay between oxygen vacancies and Ag–CeO_2 interaction in Ag/CeO_2 catalysts and their influence on the catalytic activity, J. Catal. 293 (2012) 195–204, https://doi.org/10.1016/j.jcat.2012.06.025.
[47] Z. Qu, F. Yu, X. Zhang, Y. Wang, J. Gao, Support effects on the structure and catalytic activity of mesoporous Ag/CeO_2 catalysts for CO oxidation, Chem. Eng. J. 229 (2013) 522–532, https://doi.org/10.1016/j.cej.2013.06.061.
[48] P. Bera, K.C. Patil, M.S. Hegde, N.O. Reduction, CO and Hydrocarbon Oxidation over combustion synthesized Ag/CeO_2 catalyst, Phys. Chem. Chem. Phys. 2 (2000) 3715–3719, https://doi.org/10.1039/B003908J.
[49] T. Kayama, K. Yamazaki, H. Shinjoh, Nanostructured ceria-silver synthesized in a one-pot redox reaction catalyzes carbon oxidation, J. Am. Chem. Soc. 132 (2010) 13154–13155, https://doi.org/10.1021/ja105403x.
[50] K. Shimizu, H. Kawachi, A. Satsuma, Study of active sites and mechanism for soot oxidation by silver-loaded Ceria catalyst, Appl. Catal. B Environ. 96 (2010) 169–175, https://doi.org/10.1016/j.apcatb.2010.02.016.
[51] E. Aneggi, J. Llorca, C. de Leitenburg, G. Dolcetti, A. Trovarelli, Soot combustion over silver-supported catalysts, Appl. Catal. B Environ. 91 (2009) 489–498, https://doi.org/10.1016/j.apcatb.2009.06.019.
[52] C. Lee, Joo-Il Park, Y.-G. Shul, H. Einaga, Y. Teraoka, Ag supported on electrospun macro-structure CeO_2 fibrous mats for diesel soot oxidation, Appl. Catal. B Environ. 174 (2015) 185–192, https://doi.org/10.1016/j.apcatb.2015.03.008.
[53] M. Machida, Y. Murata, K. Kishikawa, D. Zhang, K. Ikeue, On the reasons for high activity of CeO_2 catalyst for soot oxidation, Chem. Mater. 20 (2008) 4489–4494, https://doi.org/10.1021/cm800832w.
[54] K. Yamazaki, T. Kayama, F. Dong, H. Shinjoh, A mechanistic study on soot oxidation over CeO_2–Ag catalyst with 'rice-ball' morphology, J. Catal. 282 (2011) 289–298, https://doi.org/10.1016/j.jcat.2011.07.001.
[55] M.V. Grabchenko, G.V. Mamontov, V.I. Zaikovskii, V. La Parola, L.F. Liotta, O.V. Vodyankina, Design of Ag-CeO_2/SiO_2 catalyst for oxidative dehydrogenation of ethanol: control of Ag–CeO_2 interfacial interaction, Catal. Today (2018), https://doi.org/10.1016/j.cattod.2018.05.014 In Press.
[56] G.V. Mamontov, M.V. Grabchenko, V.I. Sobolev, V.I. Zaikovskii, O.V. Vodyankina, Ethanol dehydrogenation over Ag-CeO_2/SiO_2 catalyst: role of Ag-CeO_2 interface, Appl. Catal. A Gen. 528 (2016) 161–167, https://doi.org/10.1016/j.apcata.2016.10.005.
[57] M.V. Grabchenko, G.V. Mamontov, V.I. Zaikovskii, O.V. Vodyankina, Effect of the metal − support interaction in Ag/CeO_2 catalysts on their activity in ethanol oxidation, Kinet. Catal. 58 (2017) 642–648, https://doi.org/10.1134/S0023158417050056.
[58] T. Mitsudome, Y. Mikami, M. Matoba, T. Mizugaki, K. Jitsukawa, K. Kaneda, Design of a Silver–Cerium Dioxide Core–Shell Nanocomposite Catalyst for Chemoselective Reduction Reactions, Angew. Chem. Int. Ed. 51 (2012) 136–139, https://doi.org/10.1002/anie.201106244.
[59] J. Zhang, L. Li, X. Huang, G. Li, Fabrication of Ag–CeO_2 core–shell nanospheres with enhanced catalytic performance due to strengthening of the interfacial interactions, J. Mater. Chem. 22 (2012) 10480–10487, https://doi.org/10.1039/C2JM16701H.
[60] G.K. Bokii, Kristallokhimiya (Crystal Chemistry), Nauka, Moscow, 1971.
[61] L. Ma, D. Wang, J. Li, B. Bai, L. Fu, Y. Li, Ag/CeO_2 nanospheres: Efficient catalysts for formaldehyde oxidation, Appl. Catal. B Environ. 148–149 (2014) 36–46, https://doi.org/10.1016/j.apcatb.2013.10.039.
[62] T. Montini, M. Melchionna, M. Monai, P. Fornasiero, Fundamentals and catalytic applications of CeO_2-Based materials, Chem. Rev. 116 (2016) 5987–6041, https://doi.org/10.1021/acs.chemrev.5b00603.
[63] P. Burroghs, A. Hammett, A.F. Archard, G. Thornton, Satellite structure in the X-ray photoelectron spectra of some binary and mixed oxides of lanthanum and cerium, J. Chem. Soc. Dalton Trans. (1976) 1686–1698, https://doi.org/10.1039/DT9760001686.
[64] E.J. Preisler, O.J. Marsh, R.A. Beach, T.C. McGill, Stability of cerium oxide on silicon studied by x-ray photoelectron spectroscopy, J. Vac. Sci. Technol. B 19 (2001) 1611–1618, https://doi.org/10.1116/1.1387464.
[65] A.V. Naumkin, A. Kraut-Vass, S.W. Gaarenstroom, C.J. Powell, NIST Standard Reference Database 20, Version 4.1 Web Version, https://srdata.nist.gov/xps/.
[66] A. Barrie, N. Christensen, High-resolution X-ray photoemission spectra of silver, Phys. Rev. B 14 (1976) 2442–2446, https://doi.org/10.1103/PhysRevB.14.2442.
[67] T.F. Moulder, W.J. Stickle, P.E. Sobol, K.D. Bomben, Handbook of X-ray Photoelectron Spectroscopy, Perkin Elmer, Eden Prairie, Minnesota, 1992.
[68] V.K. Kaushik, XPS core level spectra and Auger parameters for some silver compounds, J. Electron. Spectrosc. Relat. Phenom. 56 (1991) 273–277, https://doi.org/10.1016/0368-2048(91)85008-H.
[69] C. Lee, J. Park, Y. Shul, H. Einaga, Y. Teraoka, Ag supported on electrospun macro-structure CeO_2 fibrous mats for diesel soot oxidation, Appl. Catal. B Environ. 174 (2015) 185–192, https://doi.org/10.1016/j.apcatb.2015.03.008.
[70] D.D. Kong, G.D. Wang, Y.H. Pan, S.W. Hu, J.B. Hou, H.B. Pan, C.T. Campbell, J.F. Zhu, Growth, structure, and stability of Ag on CeO_2 (111): synchrotron radiation photoemission studies, J. Phys. Chem. C 115 (2011) 6715–6725, https://doi.org/10.1021/jp112392y.
[71] G.K. Wertheim, S.B. DiCenzo, Cluster growth and core-electron binding energies in supported metal clusters, Phys. Rev. B 37 (1988) 844–847, https://doi.org/10.1103/PhysRevB.37.844.
[72] M.G. Mason, Electronic structure of supported small metal clusters, Phys. Rev. B 27 (1983) 748–762, https://doi.org/10.1103/PhysRevB.27.748.
[73] S. Zhang, Z. Xia, T. Ni, Z. Zhang, Y. Ma, Y. Qu, Strong electronic metal-support interaction of Pt/CeO_2 enables efficient and selective hydrogenation of quinolines at room temperature, J. Catal. 359 (2018) 101–111, https://doi.org/10.1016/j.jcat.2018.01.004.
[74] F. Yang, J. Huang, T. Odoom-Wubah, Y. Hong, M. Du, D. Sun, L. Jia, Q. Li, Efficient Ag/CeO_2 catalysts for CO oxidation prepared with microwave-assisted biosynthesis, Chem. Eng. J. 269 (2015) 105–112, https://doi.org/10.1016/j.cej.2015.01.062.
[75] M. Habibi, R. Sheibani, Preparation and characterization of nanocomposite ZnO–Ag thin film containing nano-sized Ag particles: influence of preheating, annealing temperature and silver content on characteristics, J. Solgel Sci. Technol. 54 (2010) 195–202 https://doi.org/10.1007%2Fs10971-010-2177-x.
[76] A.M. Ferraria, A.P. Carapeto, A.M. Botelho do Rego, X-ray photoelectron spectroscopy: silver salts revisited, Vacuum 86 (2012), https://doi.org/10.1016/j.vacuum.2012.05.031 1988-1921.
[77] G.I.N. Waterhouse, G.A. Bowmaker, J.B. Metson, Interaction of a polycrystalline silver powder with ozone, Surf. Interface Anal. 33 (2002) 401–409, https://doi.org/10.1002/sia.1223.
[78] L.S. Kibis, D.A. Svintsitskiy, T.Y. Kardash, E.M. Slavinskaya, E.Y. Gotovtseva, V.A. Svetlichnyi, A.I. Boronin, Interface interactions and CO oxidation activity of Ag/CeO_2 catalysts: a new approach using model catalytic systems, Appl. Catal. A Gen. 570 (2019) 51–61, https://doi.org/10.1016/j.apcata.2018.11.005.
[79] X. Wang, Z. Jiang, B. Zheng, Z. Xie, L. Zheng, Synthesis and shape-dependent catalytic properties of CeO_2 nanocubes and truncated octahedra, CrystEngComm 14 (2012) 7579–7582, https://doi.org/10.1039/C2CE25333J.
[80] S. Liu, X. Wu, W. Liu, W. Chen, R. Ran, M. Li, D. Weng, Soot oxidation over CeO_2 and Ag/CeO_2: factors determining the catalyst activity and stability during reaction, J. Catal. 337 (2016) 188–198, https://doi.org/10.1016/j.jcat.2016.01.019.
[81] Z. Wu, S.H. Overbury, Catalysis by materials with well-defined structures, Elsevier Inc. (2015) 44–45.
[82] B.M. Reddy, G.K. Reddy, L. Katta, Structural characterization and dehydration activity of CeO_2–SiO_2 and CeO_2–ZrO_2 mixed oxides prepared by a rapid microwave-assisted combustion synthesis method, J. Mol. Catal. A Chem. 319 (2010) 52–57, https://doi.org/10.1016/j.molcata.2009.11.020.
[83] S. Deshpande, S. Patil, S. Kuchibhatla, S. Seal, Size dependency variation in lattice parameter and valency states in nanocrystalline cerium oxide, Appl. Phys. Lett. 87 (2005) 133113, , https://doi.org/10.1063/1.2061873.
[84] J.M. López, A.L. Gilbank, T. García, B. Solsona, S. Agouram, L. Torrente-Murciano, The prevalence of surface oxygen vacancies over the mobility of bulk oxygen in nanostructured ceria for the total toluene oxidation, Appl. Catal. B Environ. 174–175 (2015) 403–412, https://doi.org/10.1016/j.apcatb.2015.03.017.
[85] Z.L. Wu, M.J. Li, J. Howe, H.M. Meyer, S.H. Overbury, Probing defect sites on CeO_2 nanocrystals with well-defined surface planes by Raman spectroscopy and O_2 adsorption, Langmuir 26 (2010) 16595–16606, https://doi.org/10.1021/la101723w.
[86] Y. Kang, M. Sun, A. Li, Studies of the catalytic oxidation of CO over Ag/CeO_2 catalyst, Catal. Lett. 142 (2012) 1498–1504, https://doi.org/10.1007/s10562-012-0893-2.
[87] J. Guzman, S. Carrettin, A. Corma, $_2$Spectroscopic evidence for the supply of reactive oxygen during CO oxidation catalyzed by gold supported on nanocrystalline CeO, J. Am. Chem. Soc. 127 (2005) 3286–3287 https://doi.org/ 10.1021/ja043752s.
[88] V.V. Pushkarev, V.I. Kovalchuk, J.L. d'Itri, Probing defect sites on the CeO_2 surface with dioxygen, J. Phys. Chem. B 108 (2004) 5341–5348, https://doi.org/10.1021/jp0311254.
[89] H. Wang, S. Liu, Z. Zhao, X. Zou, M. Liu, W. Liu, X. Wu, D. Weng, Activation and deactivation of Ag/CeO_2 during soot oxidation: influences of interfacial ceria reduction, Catal. Sci. Technol. 7 (2017) 2129–2139, https://doi.org/10.1039/C7CY00450H.
[90] T. Naganuma, E. Traversa, Stability of the Ce^{3+}valence state in cerium oxide nanoparticle layers, Nanoscale 4 (2012) 4950–4953, https://doi.org/10.1039/C2NR30406F.
[91] A.I.Y. Tok, S.W. Du, F.Y.C. Boey, W.K. Chong, Hydrothermal synthesis and characterization of rare earth doped ceria nanoparticles, Mater. Sci. Eng. A 466 (2007) 223–229, https://doi.org/10.1016/j.msea.2007.02.083.
[92] Y. Lee, G. He, A.J. Akey, R. Si, M. Flytzani-Stephanopoulos, I.P. Herman, Raman Analysis of Mode Softening in Nanoparticle $CeO_{2-}\delta$ and Au-$CeO_{2-}\delta$ during CO Oxidation, J. Am. Chem. Soc. 133 (2011) 12952–12955, https://doi.org/10.1021/ja204479j.
[93] A. Trovarelli, Catalytic properties of Ceria and CeO_2-Containing materials, Catal. Rev. 38 (1996) 439–520, https://doi.org/10.1080/01614949608006464.
[94] K. Krishna, A. Bueno-López, M. Makkee, J. Moulijn, Potential rare earth modified CeO_2 catalysts for soot oxidation: I. Characterisation and catalytic activity with O_2, Appl. Catal. B Environ. 75 (2007) 189–200, https://doi.org/10.1016/j.apcatb.2007.04.010.
[95] M. Liu, X. Wu, S. Liu, Y. Gao, Z. Chen, Y. Ma, R. Ran, D. Weng, Study of Ag/CeO_2 catalysts for naphthalene oxidation: balancing the oxygen availability and oxygen regeneration capacity, Appl. Catal. B Environ. 219 (2017) 231–240, https://doi.org/10.1016/j.apcatb.2017.07.058.
[96] G.V. Mamontov, V.V. Dutov, V.I. Sobolev, O.V. Vodyankina, Effect of transition metal oxide additives on the activity of an Ag/SiO_2 catalyst in carbon monoxide oxidation, Kinet. Catal. 54 (4) (2013) 487–491, https://doi.org/10.1134/S0023158413040137.
[97] Z. Qu, W. Huang, M. Cheng, X. Bao, Restructuring and redispersion of silver on

SiO_2 under oxidizing/reducing atmospheres and its activity toward CO oxidation, J. Phys. Chem. B 109 (2005) 15842–15848, https://doi.org/10.1021/jp050152m.
[98] L. Yu, R. Peng, L. Chen, M. Fu, J. Wu, D. Ye, Ag supported on CeO_2 with different morphologies for the catalytic oxidation of HCHO, Chem. Eng. J. 334 (2018) 2480–2487, https://doi.org/10.1016/j.cej.2017.11.121.
[99] K. Wu, L. Zhou, C.-J. Ji, L.-D. Sun, C.-H. Yan, Pt-embedded-CeO_2 hollow spheres for enhancing CO oxidation performance, Mater. Chem. Front.1 (2017) 1754–1763, https://doi.org/10.1039/C7QM00244K.
[100] D. Fino, N. Russo, G. Saracco, V. Specchia, The role of suprafacial oxygen in some perovskites for the catalytic combustion of soot, J. Catal. 217 (2003) 367–375, https://doi.org/10.1016/S0021-9517(03)00143-X.
[101] L.F. Liotta, M. Ousmane, G. Di Carlo, G. Pantaleo, G. Marcì, L. Retailleau, A. Giroir-Fendler, Total oxidation of propene at low temperature over Co_3O_4–CeO_2 mixed oxides: role of surface oxygen vacancies and bulk oxygen mobility in the catalytic activity, Appl. Catal. A Gen. 347 (2008) 81–88, https://doi.org/10.1016/j.apcata.2008.05.038.
[102] C. Aliotta, L.F. Liotta, V. La Parola, A. Martorana, E.N.S. Muccillo, R. Muccillo, F. Deganello, Ceria-based electrolytes prepared by solution combustion synthesis: the role of fuel on the materials properties, Appl. Catal. B: Environ. 197 (2016) 14–22, https://doi.org/10.1016/j.apcatb.2016.02.044.
[103] G. Li, X. Zhang, W. Feng, X. Fang, J. Liu, Nanoporous CeO_2-Ag catalysts prepared by etching the CeO_2/CuO/Ag_2O mixed oxides for CO oxidation, Corros. Sci. 134 (2018) 140–148, https://doi.org/10.1016/j.corsci.2018.02.029Get rights and content.
[104] V.V. Dutov, G.V. Mamontov, V.I. Zaikovskii, O.V. Vodyankina, The effect of support pretreatment on activity of Ag/SiO_2 catalysts in low-temperature CO oxidation, Catal, Today 278 (2016) 150–156, https://doi.org/10.1016/j.cattod.2016.05.033.
[105] E. Kolobova, Y. Kotolevich, E. Pakrieva, G. Mamontov, M.H. Farias, V. Cortés Corberán, N. Bogdanchikova, J. Hemming, A. Smeds, P. Mäki-Arvela, D.Y. Murzin, A. Pestryakov, Modified Ag/TiO_2 systems: promising catalysts for liquid-phase oxidation of alcohols, Fuel 234 (2018) 110–119, https://doi.org/10.1016/j.fuel.2018.06.128.
[106] G.B.D. Mea, L.P. Matte, A.S. Thill, F.O. Lobato, E.V. Benvenutti, L.T. Arenas, A. Jürgensen, R. Hergenröder, F. Poletto, F. Bernardi, Tuning the oxygen vacancy population of cerium oxide (CeO_{2-x}, $0 < x < 0.5$) nanoparticles, Appl. Surf. Sci. 422 (2017) 1102–1112, https://doi.org/10.1016/j.apsusc.2017.06.101.
[107] B. Bulfin, A.J. Lowe, K.A. Keogh, B.E. Murphy, O. Lübben, S.A. Krasnikov, I.V. Shvets, Analytical model of CeO_2 oxidation and reduction, J. Phys. Chem. C 117 (2013) 24129–24137, https://doi.org/10.1021/jp406578z.
[108] G. Corro, E. Vidal, S. Cebada, U. Palc, F. Banuelos, D. Vargas, E. Guilleminot, Electronic state of silver in Ag/$SiO_2$and Ag/ZnO catalysts and its effect on diesel particulate matter oxidation: An XPS study, Appl. Catal. B Environ. 216 (2017) 1–10, https://doi.org/10.1016/j.apcatb.2017.05.059.
[109] S. Wu, Y. Yang, C. Lu, Y. Ma, S. Yuan, G. Qian, Soot oxidation over CeO_2 or Ag/CeO_2: influences of bulk oxygen vacancies and surface oxygen vacancies on activity and stability of the catalyst, Eur. J. Inorg. Chem. (2018) 2944–2951, https://doi.org/10.1002/ejic.201800423.
[110] H. Wang, S. Luo, M. Zhang, W. Liu, X. Wu, S. Liu, Roles of oxygen vacancy and O_x^- in oxidation reactions over CeO_2 and Ag/CeO_2 nanorod model catalysts, J. Catal. 368 (2018) 365–378, https://doi.org/10.1016/j.jcat.2018.10.018.